Gasdermin D–mediated release of IL-33 from senescent hepatic stellate cells promotes obesity-associated hepatocellular carcinoma

RYOTA YAMAGISHI, FUMITAKA KAMACHI, MASARU NAKAMURA, SHOTA YAMAZAKI, TOMONORI KAMIYA, MASAKI TAKASUGI, YI CHENG, YOSHIKI NONAKA, YOSHIMI YUKAWA-MUTO, LE THI THANH THUY, YOHSUKE HARADA, TATSUYA ARAI, TZE MUN LOO, SHIN YOSHIMOTO, TATSUYA ANDO, MASAHIRO NAKAJIMA, HAYAO TAGUCHI, TAKAMASA ISHIKAWA, HISAYA AKIBA, SACHIKO MIYAKE, MASATO KUBO, YOICHIRO IWAKURA, SHINJI FUKUDA, WEI-YU CHEN, NORIFUMI KAWADA, ALEXANDER RUDENSKY, SUSUMU NAKAE, EIJI HARA, AND NAOKO OHTANI

Citation	SCIENCE IMMUNOLOGY. 7(72)
Issue Date	2022-06-24
Type	Journal Article
Textversion	Author
Note	This is the accepted version. The formal published version is available at https://doi.org/10.1126/sciimmunol.abl7209.
Supplementary Materials	Supplementary Materials is available at https://doi.org/10.1126/sciimmunol.abl7209.
DOI	10.1126/sciimmunol.abl7209

Highlights	◇高脂肪食の長期摂取で腸管バリアが脆弱化し、肝臓に移行・蓄積したグラム陽性腸内細菌叢の細胞壁成分であるリポタイコ酸が肝臓に移行・蓄積。 ◇肝臓に蓄積したリポタイコ酸のトル様受容体を介した刺激により、老化肝星細胞中のタンパク質・ガスダーミン D が酵素切断され、生じた N 末端側の部分が集合して細胞膜上に小孔を形成、その小孔からがんを促進する物質（IL-1β、IL-33 を含む SASP 因子）が細胞外に放出。 ◇放出された SASP 因子の IL-33 が、がん細胞に対する免疫を抑制する制御性 T 細胞（Treg 細胞）を活性化し、がんの増殖をより促進。
Description	【概要】 大阪公立大学大学院医学研究科・病態生理学の大谷直子教授、山岸良多助教を中心とするグループは、同肝胆膵病態内科学の河田則文教授、慶應義塾大学先端生命科学研究所の福田真嗣特任教授、広島大学大学院・統合生命科学研究科の中江進教授らと共同で、肝臓に移行した腸内細菌叢の成分であるリポタイコ酸が、肝がん微小環境を変化させてがんの増殖進展を促進する SASP(Senescence-associated secretory phenotype、細胞老化随伴分泌現象)因子を老化肝星細胞から放出させるメカニズムを明らかにしました。 がんの組織はがん細胞そのものだけでなく、線維芽細胞や免疫細胞など、様々な種類の細胞種が集まって「がん微小環境」を構成しています。進行したがん組織の微小環境ではがん細胞周囲の細胞ががんの増殖を助長していると考えられています。本グループは、脂肪肝を素地とする肝がん微小環境では、肝星細胞と呼ばれる線維芽細胞が細胞老化を引き起こしており、「細胞老化随伴分泌現象（SASP）」という様々な分泌因子を放出する現象が生じ、その分泌因子（SASP 因子）ががんの増殖を促進することを以前から見出していました。しかしこれまでに SASP 因子の放出メカニズムについては明らかにされていませんでした。 本研究では高脂肪食摂取による肥満誘導性肝がんのマウスモデルを用い、老化肝星細胞の細胞膜上にガスダーミン D というタンパク質が酵素切断されて生じた N 末端側の部分（以降 GSDMD－N と略記）が集合して形成される小孔を介して、SASP 因子に含まれるサイトカイン IL-1β と IL-33 が細胞の外部に放出されることを明らかにしました。また、高脂肪食摂取マウスでは、腸管バリアが脆弱化しており、肝臓にグラム陽性腸内細菌の細胞壁成分であるリポタイコ酸が蓄積していました。さらに、蓄積したリポタイコ酸は老化肝星細胞にトル様受容体２（TLR2）を介した刺激を入れ続け、酵素切断で生じた GSDMD－N による細胞膜上の小孔形成とそれに続く IL-33 や IL-1β の放出を促進していることもわかりました。老化肝星細胞から放出された IL-33 は、その受容体 ST2 が陽性の制御性 T 細胞（Treg 細胞）に作用し、がんの増殖を促進させることがわかりました。また、GSDMD－N はヒトの NASH（Non-alcoholic steatohepatitis）肝がんの腫瘍部にある肝星細胞でもその存在が認められました。これらの結果から、ガスダーミン D による小孔形成を阻害する薬剤は肝がんの予防や治療につながる可能性があります。

‘脂肪肝による肝がんの進行が腸内細菌によって促進されるメカニズムの一端を解明’．大阪公立大学. https://www.omu.ac.jp/info/research_news/entry-01214.html. （参照 2022-06-25）

Gasdermin D-mediated release of IL-33 from senescent hepatic stellate cells promotes obesity-associated hepatocellular carcinoma

Ryota Yamagishi[1,23], Fumitaka Kamachi[1,2,23], Masaru Nakamura[2], Shota Yamazaki[2], Tomonori Kamiya[1], Masaki Takasugi[1], Yi Cheng[1], Yoshiki Nonaka[3], Yoshimi Yukawa-Muto[1,4], Le Thi Thanh Thuy[4], Yohsuke Harada[5], Tatsuya Arai[2], Tze Mun Loo[2,6], Shin Yoshimoto[6], Tatsuya Ando[2], Masahiro Nakajima[2], Hayao Taguchi[2], Takamasa Ishikawa[7], Hisaya Akiba[8], Sachiko Miyake[8], Masato Kubo[9,10], Yoichiro Iwakura[11],Shinji Fukuda[7,12,13], Wei-Yu Chen[14,15], Norifumi Kawada[4], Alexander Rudensky[16], Susumu Nakae[17,18], Eiji Hara[19,20,21], and Naoko Ohtani [1,2,22,*]

[1] Department of Pathophysiology, Osaka Metropolitan University, Graduate School of Medicine, Osaka, Japan (formerly, Osaka City University)
[2] Department of Applied Biological Science, Faculty of Science and Technology, Tokyo University of Science, Noda, Chiba, Japan
[3] Department of Pathophysiology, Osaka City University, Graduate School of Medicine, Osaka, Japan
[4] Department of Hepatology, Osaka Metropolitan University, Graduate School of Medicine, Osaka, Japan (formerly, Osaka City University)
[5] Laboratory of Pharmaceutical Immunology, Faculty of Pharmaceutical Sciences, Tokyo University of Science, Noda, Chiba, Japan
[6] Cancer Institute, Japanese Foundation for Cancer Research, Koto-ku, Tokyo, Japan
[7]Institute for Advanced Biosciences, Keio University, Tsuruoka, Yamagata, Japan.
[8] Department of Immunology, Juntendo University School of Medicine, Tokyo, Japan
[9] Division of Molecular Pathology, Research Institute for Biomedical Science, Tokyo University of Science, Noda, Chiba, Japan
[10] Laboratory for Cytokine Regulation, Research Center for Integrative Medical Science (IMS), RIKEN Yokohama Institute, Yokohama, Kanagawa, Japan
[11] Center for Animal Disease Models, Research Institute for Biomedical Sciences, Tokyo University of Science, Noda-shi, Chiba, Japan
[12]Gut Environmental Design Group, Kanagawa Institute of Industrial Science and Technology, Kawasaki, Kanagawa, Japan.
[13]Transborder Medical Research Center, University of Tsukuba, Tsukuba, Ibaraki, Japan.
[14] Institute for Translational Research in Biomedicine, Kaohsiung Chang Gung Memorial Hospital, Kaohsiung, Taiwan
[15] Department of Biochemistry and Molecular Biology, College of Medicine, National Cheng Kung University, Tainan, Taiwan.
[16]Howard Hughes Medical Institute and Immunology Program, Memorial Sloan Kettering Cancer Center, New York, NY, USA
[17]Graduate School of Integrated Sciences for Life, Hiroshima University, Higashi-Hiroshima City, Hiroshima, Japan
[18]Precursory Research for Embryonic Science and Technology (PRESTO), Japan Science and Technology Agency, Saitama, Japan
[19]Research Institute for Microbial Diseases, Osaka University, Suita, Osaka, Japan.
[20]Immunology Frontier Research Center (IFReC) Osaka University, Suita, Osaka, Japan.
[21]Center for Infectious Disease Education and Research (CiDER), Osaka University, Suita, Japan.
[22]AMED-CREST, Japan Agency for Medical Research and Development, Tokyo, Japan
[23] These authors contributed equally to this work
*Correspondence: naoko.ohtani@omu.ac.jp

Single sentence summary:

We clarified the release mechanism of SASP factors via gasdermin D N-terminus cell membrane pore from senescent hepatic stellate cells.

Abstract

Long-term senescent cells exhibit a secretome termed the senescence-associated secretory phenotype (SASP). Although the mechanisms of SASP factor induction have been intensively studied, the release mechanism and how SASP factors influence tumorigenesis in the biological context remains unclear. In this study, using a mouse model of obesity-induced hepatocellular carcinoma (HCC), we identified the release mechanism of SASP factors, that include IL-1β and IL-1β-dependent IL-33, from senescent hepatic stellate cells via gasdermin D (GSDMD) N-terminus-mediated pore. We found that IL-33 was highly induced in senescent hepatic stellate cells (HSCs) in an IL-1β-dependent manner in the tumor microenvironment. The release of both IL-33 and IL-1β was triggered by lipoteichoic acid (LTA), a cell wall component of gut microbiota which was transferred and accumulated in the liver tissue of high fat diet fed mice, and the release of these factors was mediated through cell membrane pores formed by the gasdermin D (GSDMD) N-terminus, which was cleaved by LTA-induced caspase-11. We demonstrated that IL-33 release from HSCs promoted HCC development via the activation of ST2-positive Treg cells in the liver tumor microenvironment. The accumulation of GSDMD N-terminus was also detected in HSCs from human NASH-associated HCC patients, suggesting that similar mechanism could be involved in a certain type of human HCC. These results uncover a release mechanism for SASP factors from sensitized senescent HSCs in the tumor microenvironment, thereby facilitating obesity-associated HCC progression. Furthermore, our findings highlight the therapeutic potential of inhibitors of GSDMD-mediated pore formation for HCC treatment.

Introduction

Cellular senescence is a state of permanent cell cycle arrest that is induced by various cellular stresses including persistent DNA damage and is known to function as a tumor-suppression mechanism (*1*). However, although senescent cells cease proliferating, they express a variety of secreted proteins, such as inflammatory cytokines, chemokines, proteases, and so on, and this phenotype is called the senescence-associated secretory phenotype (SASP)(*1-4*). Our previous studies and other researches elucidated the transcriptional and translational mechanisms of SASP factor induction (*1, 5*), and more recently, cGAS-STING-mediated signaling (*1, 6*) was shown to be crucial for intrinsic SASP induction. However, the interactions of multiple SASP factors and their release mechanism have not been clarified particularly when a series of factors are simultaneously produced in senescent cells.

Nonalcoholic fatty liver disease (NAFLD) and nonalcoholic steatohepatitis (NASH) are increasingly recognized as a risk of HCC development, independently of cirrhosis (*7*). Using the murine NASH-associated liver cancer model, which is less fibrotic, we previously identified that the exposure to deoxycholic acid (DCA), a circulating secondary bile acid produced by gut microbiota, provoked cellular senescence and SASP in hepatic stellate cells (HSCs) in the liver (*8, 9*), playing a role as cancer-associated fibroblasts (CAFs) exhibiting an oncogenic secretome in the tumor microenvironment (*2*). We also previously reported that this tumor-promoting secretome is triggered by lipoteichoic acid (LTA), a cell wall component of gram-positive bacteria, suppressed anti-tumor immunity via PGE_2 overproduction in the senescent HSCs in the liver tumor region, which was canceled in the mice lacking TLR2, an innate immune receptor recognizing LTA (*9*). This tumor-promoting SASP phenotype of HSCs was

observed in the human NASH-associated HCC tumor area (*8, 9*). In our obesity-associated liver cancer model, we found that a variety of SASP factors are expressed in the HSCs in the liver tumor, and IL-1β, an upstream regulator of cytokine cascade, plays an important role in hepatocellular carcinoma (HCC) development, although the downstream tumorigenic cytokines are still unknown (*8*). We, therefore, focused on IL-33 which is highly expressed in HSCs in an IL-1β-dependent manner.

IL-33 is an IL-1 family cytokine that can act through its receptor, ST2(IL-1RL1) and IL-1RAcP (*10, 11*), on various types of immune cells (*10, 12*). IL-33 is expressed in many types of cells, such as epithelial cells, endothelial cells, and fibroblasts, and is released by cellular damage as an alarmin to provoke immune responses (*10, 13*). In addition, IL-33 is processed by serine proteases secreted by myeloid cells that can cleave full-length IL-33 (35 kDa) into mature forms (18–21 kDa) whose activity is much greater than that of full-length IL-33 (*10, 14, 15*). Although IL-33 was initially identified as an allergy-associated cytokine(*10, 13, 16*), it has been increasingly recognized as a tumor-promoting cytokine in several types of cancer(*17-21*). However, when focusing on the liver, the precise molecular mechanisms of how naturally produced endogenous IL-33 contributes to HCC development is still incompletely understood (*22-24*).

In this study, we found that IL-33, an IL-1β-dependent SASP factor, was upregulated in senescent hepatic stellate cells (HSCs) in the obesity-associated liver tumor microenvironment, and cleaved by chymotrypsin-like elastase family member 1 (CELA1). Interestingly, lipoteichoic acid (LTA) was highly accumulated in the obese mouse liver due to gut barrier dysfunction, and the short and active forms of IL-1β and IL-33 were found to be released from LTA-stimulated senescent HSCs via the cell

membrane pore formed by the gasdermin D (GSDMD) N-terminus (*25*), which was cleaved by caspase-11. The active form of IL-33 released from HSCs stimulated ST2-positive Treg cells to suppress antitumor immunity.

Results

IL-33 from senescent HSCs promotes obesity-associated HCC development

We have previously reported that IL-1β, an upstream regulator of cytokine cascade, plays an important role in hepatocellular carcinoma (HCC) development (*8*). To explore which SASP factors from senescent HSCs in the tumor microenvironment downstream of IL-1β are involved in obesity-associated HCC development, we investigated the expression of a series of inflammatory cytokines produced in the liver tumor tissue. Microarray analysis showed that IL-33 was the most upregulated cytokine in the tumor tissue compared with non-tumor tissue in the livers of DMBA-treated, high-fat diet (HFD)-fed mice (Fig. 1A and 1B). The quantitative PCR analysis confirmed that IL-33 mRNA was indeed highly expressed in the tumor tissue (Fig. 1C). Interestingly, not only the full-length IL-33 but also the short form of IL-33, which is known to be more active (*14*), were highly expressed specifically in the tumor tissue (Fig. 1D). Therefore, to investigate the role of IL-33 in obesity-associated HCC development, IL-33-deficient mice (*26*) were treated with DMBA in the neonatal stage and fed an HFD to develop chemically-induced HCC as previously described (*8, 9*). Interestingly, the IL-33-deficient mice showed a statistically significant reduction of liver tumor development in number and size compared with the wild-type mice, although the body weights of the mice were unchanged between the two groups (Fig. 1E and 1F). Conversely, the administration of recombinant IL-33 into wild-type mice

promoted HCC development without influencing body weight (Fig. 1E and 1G). Notably, histological analysis revealed that IL-33 was highly expressed in α-smooth muscle actin (α-SMA)-positive HSCs in the tumor microenvironment undergoing cellular senescence, as judged by the expression of a senescence inducer, p21 (a cyclin-dependent kinase inhibitor, CDKI), signs of DNA damage response (53BP1 foci), and suppressed expression of the cell proliferation marker (negative expression of Ki-67) (Fig. 1H) (*1, 8*). HFD-fed livers showed a higher number of senescent HSCs expressing p21 than ND-fed livers, coinciding with the upregulation of SASP factors, IL-33, and IL-1β in senescent HSCs (Fig. S1).

We have previously shown that DCA, an obesity-associated gut microbial metabolite, has a pivotal role in inducing DNA damage-associated cellular senescence and concomitant SASP in HSCs, thereby contributing to HCC progression (*8, 9*). DCA treatment in primary HSCs indeed upregulated the expression of senescence inducing CDKIs, p16, and p21 (Fig. 2D)(*8, 9*). Therefore, we checked the effect of DCA on the induction of cellular senescence and IL-33 expression in HSCs *in vivo*. Although the number of 53BP1foci, a marker of DNA-damage-induced cellular senescence, in HSCs was significantly reduced in the livers of four antibiotics (4Abx)-treated mice (Fig. 2A, vi; Fig. 2C), the foci number were strongly increased by the 4Abx plus DCA-feeding (Fig. 2A, vii; Fig. 2C), indicating that DNA damage response was induced by DCA *in vivo*. The number of IL-33-expressing α-SMA-positive HSCs was very few in the 4Abx-treated livers (Fig. 2A, ii; Fig. 2B). However, upon DCA-feeding, the IL-33 expression was increased coinciding with the accumulation of the DNA damage response marker, 53BP1 foci (Fig. 2A, iii and vii; Fig. 2B, and 2C). We previously showed that IL-1β-deficient mice had a significant reduction in the development of

HFD-induced HCCs (*8*). Accordingly, we found that the number of IL-33-positive HSCs was also greatly decreased in mice lacking IL-1β (Fig. 2A, iv; Fig. 2B)(*27*), which is an important upstream cytokine for SASP factor induction (*8*), suggesting that *Il33* expression could be regulated by IL-1β. When DCA-induced senescent HSCs were treated with IL-1β in culture, *Il33* mRNA level was strongly enhanced by IL-1β stimulation compared to the response in non-senescent HSCs treated with vehicle (Fig. 2D). Similar enhancement of *Cxcl1* mRNA induction, a well-known SASP factor (*8*), was observed in DCA-treated senescent HSCs by IL-1β addition (Fig. 2D). DCA treatment increased the mRNA levels of the senescence-inducing CDKIs, p16, and p21, but this upregulation did not respond to IL-1β treatment (Fig. 2D).

IL-33 is cleaved and activated by the elastase, CELA1

We next tried to elucidate the molecular mechanism of IL-33 activation in senescent HSCs in the tumor microenvironment. First, we focused on the mechanism of how the short and active form of IL-33 was created in the obesity-associated liver tumor microenvironment (Fig. 1D). It is known that the short form of C-terminal IL-33, which is generated by the proteolytic cleavage of full-length IL-33 by serine proteases to eliminate the N-terminal chromatin binding domain (CBD), has an enhanced biological activity (*14, 15*). Microarray analysis showed that CELA1, but none of the other known IL-33-processing proteases (Cathepsin G, Neutrophil elastase, Granzyme B, Tryptase, Chymase, or Calpain-1) (*14, 15, 28*), was highly expressed in the tumor tissue compared to that in the non-tumor tissue in HFD-fed mouse livers (Fig. 3A and 3B). We confirmed that the protein, as well as mRNA levels of CELA1, were very high in the tumor region (Fig. 3C and 3D), and more interestingly, CELA1 was also predominantly

expressed in α-SMA-positive senescent HSCs in the area of the liver tumor (Fig. 3E). To investigate whether CELA1 can cleave the full-length IL-33 to generate the short form, the recombinant full-length IL-33 was mixed with recombinant CELA1 *in vitro*. We found that recombinant CELA1 exhibited IL-33-processing activity and was able to create shorter forms of IL-33 (Fig. 3F), while an elastase inhibitor, elastatinal, blocked the cleavage of IL-33 by CELA1 (Fig. 3F). Consistent with CELA1 upregulation in HSCs in the liver tumor tissue (Fig. 3E), CELA1 mRNA was increased in DCA-induced senescent HSCs, although CELA1 expression was IL-1β-independent (Fig. 3G).

To investigate the IL-33 cleavage by CELA1 *in vivo*, we performed the peritoneal injection of elastatinal for five weeks at the late stage of the hepatocarcinogenesis protocol in mice (Fig. 3H). Interestingly, we confirmed a decreased production of the short form of IL-33 and an increased level of the full-length IL-33, particularly in the liver tumor region (Fig. 3I, comparison between lanes 3 and 4, and lanes 7 and 8), coinciding with the suppression of HCC development in mice administered with elastatinal (Fig. 3J), without any weight loss (Fig. 3J). The expression levels of other proteases that can reportedly cleave IL-33 seemed quite low (Fig. 3B). Therefore, these results strongly suggest that CELA1 is a protease that can cleave the full-length IL-33, contributing to the creation of a short and active form of IL-33.

IL-33 is released through the GSDMD N-terminus pore in HSCs of HFD-fed livers

Thereafter, we investigated how the cleaved form of IL-33 is exported from living senescent HSCs. To evaluate the *in vivo* status of HSCs, we freshly isolated primary HSCs from the livers of ND-fed mice or tumor-bearing HFD-fed mice by cell sorting using a modified method of previous reports (*29, 30*). The HSCs isolated from

HFD-fed murine liver tumors showed a senescent phenotype judging from the reduced proliferation ability and the increased senescence-associated β-galactosidase (SA-β gal) activity (Fig. S2A-S2C). The mRNA level of senescence inducing CDKIs, *p16* and *p21*, as well as the SASP factors, *Cxcl1, Il33, Mmp-1*, *Mmp-3,* and IL-1β receptor, *Il1r1* in the HSCs isolated from the tumor region of HFD-fed mouse livers were upregulated (Fig. S2E-S2K). We also confirmed the decreased protein level of lamin B1 in HSCs from HFD-fed liver tumors (Fig. 4B), which is one of the hallmarks of cellular senescence, creating a fragile nuclear membrane (*31*). This shows that the HSCs freshly isolated from HFD-fed liver tumor tissues were indeed undergoing cellular senescence and SASP due to sufficient exposure of endogenous DCA increased in HFD-fed mice *in vivo* (Fig.4 D) (*8*).

Using freshly prepared HSC lysates, we observed that IL-33 was most highly expressed in HSCs from tumor tissues of HFD-fed mouse livers, confirming the results presented earlier (Fig. 1D; Fig. 4A). Recently, it has been reported that IL-1β is exported from living macrophages through the cell membrane pore formed by the gasdermin D (GSDMD) N-terminus in a caspase 1 or -11 dependent manner (*32*); however, GSDMD-mediated IL-1β release from non-immune cells has not been well known. Interestingly, the cleaved form of caspase-1 and -11 were upregulated in freshly isolated HSCs from HFD-fed mouse livers and were co-expressed with both the full-length and the cleaved form of GSDMD (Fig. 4A). These findings led us to hypothesize that GSDMD in the senescent HSCs could be cleaved by caspase-1 or -11 in the tumor tissue, leading to the pore formation in the cell membrane of HSCs by the GSDMD N-terminus to export SASP factors. It is well known that microbe-associated molecular patterns (MAMPs), such as lipopolysaccharides (LPSs) or lipoteichoic acid (LTA),

activate the inflammasome pathway that can cleave and activate caspase-1 and -11 (*33*). Using the same hepatic carcinogenesis model, we previously found that the population of gram-positive gut microbiota was greatly increased in the intestine of HFD-fed mice, and a large amount of LTA, a cell wall component of gram-positive bacteria, was transferred to the liver due to the HFD-induced gut barrier dysfunction (*9, 34*). Moreover, we reported that the mice lacking TLR2, an innate immune receptor recognizing LTA, developed a significantly reduced number of HCC tumors(*9*). In this study, we also confirmed the LTA accumulation in the hepatic sinusoidal area of the HFD-fed mouse liver including in the tumor area in WT and IL-33 deficient mice, and that this accumulation was strongly diminished in the antibiotics-treated mouse liver, showing the gut barrier dysfunction supported by the elevation of serum CD14 level (Fig. S3A) and that the hepatic LTA was derived from gram-positive gut microbiota (Fig. 4C, Fig. S3B). Therefore, to mimic the biological context of this HFD-fed mouse liver, we freshly isolated HSCs from HFD-induced liver tumors and treated them with LTA as a stimulatory MAMP in culture. We noticed that the expression of IL-33, caspase-11, and GSDMD-N-terminus in HSCs was reduced in the following two-days culture compared to those in immediately prepared fresh cell lysates presumably due to culture stress (Fig. 4A, lane 3; Fig. 4B, lane 3). However, the LTA treatment strongly recovered the expression of these proteins as well as that of full-length IL-1β (Fig. 4B). Moreover, Toll-like receptor 2 (TLR2), an innate immune receptor recognizing LTA, was also highly upregulated (Fig. 4B, lane 4), suggesting that LTA and TLR2 signaling cooperate in a positive feedback loop to induce the expression of IL-1β and its downstream targets, IL-33, as well as caspase-11 (Fig. 4B, lane 4). Interestingly, we also found that LTA treatment resulted in the cleaved form of IL-1β and IL-33 being fully exported from the

HSCs into the culture supernatant, coinciding with an increase in expression of the GSDMD N-terminus domain (Fig. 4B, lane 4). The upregulation of these proteins by LTA was much weaker in HSCs from ND-fed mouse livers (Fig. 4B, lane 2), indicating that the senescent HSCs isolated from HFD-fed mouse liver tumors were highly sensitized to LTA.

Thereafter, we investigate whether GSDMD is involved in the release of IL-33 from the senescent HSCs. We first confirmed that the short form of IL-33 was released only in the presence of GSDMD N-terminus when overexpressed in HEK293T cells (Fig. 4E). We next performed the knockdown of GSDMD expression by the infection of the shRNA expression vector against the GSDMD coding sequence in isolated HSCs. In the control shRNA-infected cells, both full-length and N-terminus of GSDMD as well as IL-1β and IL-33 were highly expressed under LTA treatment (Fig. 4F, lane 1). The knockdown vector #2 and #4 successfully suppressed both the full-length and short form of GSDMD expression in the HSCs isolated from HFD-fed mouse liver tumors (Fig. 4F, lanes 2 and 3). Interestingly, the short form of endogenous IL-33 was accumulated in the cells where the expression of GSDMD was suppressed (Fig. 4F, lanes 2 and 3), indicating that the release of a short form of IL-33 from HSCs was blocked by the knockdown of GSDMD. We again confirmed the release of cleaved IL-1β from LTA-treated and control shRNA-infected HSCs in the culture supernatant, and this release was completely blocked by GSDMD knockdown (Fig. 4F, lane 2 and 3), showing that cleaved IL-1β was also released through GSDMD. The accumulation of the cleaved IL-1β in the cell lysates of senescent HSCs was under the detectable level, presumably because of its instability in MMP-induced conditions in senescent HSCs (Fig. S2I and S2J) (*35-37*). The increased sensitivity to LTA and the innate immune

responses were shown to be independent of IL-33 (Fig. 4C, Fig. S3B, and S3C). Although IL-33 is known to be a nuclear protein harboring chromatin binding domain, the production of cytoplasmic chromatin in senescent cells (*38*) due to their fragile nuclear membrane caused by downregulation of lamin B1 (Fig. 4B, lanes 3 and 4) (*31*), could result in the translocation of nuclear IL-33 to the cytoplasm where it can be cleaved by CELA1. These results strongly suggest that the cleaved form of IL-33 and IL-1β are exported through the GSDMD N-terminus pore upon LTA stimulation.

Moreover, we tried to identify the enzyme that cleaved the full-sized GSDMD in this context. Caspase-1 and -11 are capable of cleaving GSDMD (*39-41*). In the HSCs from HFD-fed liver tumors, caspase-11 was strongly upregulated upon LTA treatment, whereas the expression (Fig. 4B, lane 4) or activity (Fig. 4H) of caspase-1 was unchanged. The expression and activity of caspase-1 were sustained at a relatively high level (Fig. 4B, lanes 3 and 4), which could lead to cleaving and activating IL-1β in HSCs of HFD-fed liver tumors. When caspase-11 expression was knockdown by shRNA, GSDMD N-terminus was significantly diminished, indicating that caspase-11 cleaved GSDMD (Fig. 4G). More interestingly, TLR2 knockdown completely suppressed the induction and the processing of caspase-11 by LTA (Fig. 4I). These results strongly suggest that LTA/TLR2-mediated signaling facilitates the expression and maturation of caspase-11 leading to the creation of the GSDMD-N-terminus and the formation of the cell membrane pore as well as expression of IL-1β and IL-33 (Fig. 4I). Cell membrane pore formation by the GSDMD-N-terminus cluster is known to induce pyroptotic cell death (*25*). However, unlike LTA-treated THP1 cells, monocytic leukemia cells that are known to undergo pyroptotic cell death when treated with LPS or LTA (*25, 41*), senescent HSCs isolated from HDF-fed liver tumors seemed resistant to

pyroptotic cell death in the presence of GSDMD-N-terminus without showing any signs of cell death at least for 5 days (Fig. 4J). All these results suggest that caspase-11 upregulated by LTA cleaved the GSDMD N-terminus to create a cell membrane pore, thereby contributing to the continuous export of IL-33 and IL-1β from senescent HSCs. We believe that this constitutes an important release mechanism for the SASP factors IL-33 and IL-1β from senescent HSCs in the obesity-associated liver tumor microenvironment.

Finally, to evaluate the effect of inhibiting the SASP factor release, the DMBA-treated and HFD-fed mice were treated with disulfiram, an inhibitor of pore formation by GSDMD-N terminus(*42*), which has been originally used as a drug for treating alcohol addiction (*42*). We confirmed that disulfiram treatment indeed effectively inhibited the export of IL-1β and IL-33 from primary HSCs (Fig. S3D). Interestingly, liver tumor formation was repressed by the treatment of disulfiram (Fig. 4K), suggesting the importance of SASP factor release from HSCs on tumor formation and the promising repurposed use of disulfiram for the anti-cancer drug.

IL-33-mediated activation of ST2 positive Treg cells in the tumor microenvironment contributes to obesity-associated HCC development

To determine the target cells of IL-33 in the liver tumor microenvironment, we searched for cells expressing ST2, a receptor of IL-33, in mouse liver tissues. Since ST2 expression was not observed on the surface of HSCs, primary hepatocytes from ND-fed and HFD-fed mouse livers nor a mouse HCC cell line, Hepa1-6 cells, (Fig. 5A), we focused on immune cells. We found that ST2 was expressed predominantly on a population of Foxp3-positive regulatory $CD4^+$ T cells (hereafter designated as Treg) and

a few Foxp3-negative conventional $CD4^+$ T cells (hereafter designated as Tconv) in the HFD-fed mouse livers (Fig. 5B and 5D; Fig. S4). The frequency of $ST2^+$ Treg cells as well as total Treg cells was dominantly increased in the livers of HFD-fed mice (Fig. 5C and 5D; Fig. S4). The frequency of ST2-positive group 2 innate lymphoid cells (ILC2), which have been reportedly associated with the anti-tumor immunity (*43*), were very small in the mouse livers similar to the previous report (Fig. S5)(*44*). Therefore, we continued the analysis of ST2-positive Treg cells in the HFD-induced liver tumor. We found that the $ST2^+$ Treg cells were derived from the thymus, judging from the high expression of Helios and neuropilin-1 (*45, 46*) (Fig. 5E and 5F; Fig. S4). Molecules important for Treg cell function, such as CTLA-4(*47*) and KLRG1 (*48*) were strongly upregulated in $ST2^+$ Treg cells compared with $ST2^-$ Treg cells (Fig. 5G; Fig. S4). Thereafter, to examine the effects of IL-33 on $ST2^+$ Treg cells *in vivo*, we injected IL-33 or vehicle (PBS) intraperitoneally into HFD-fed mice. The administration of IL-33 significantly enhanced the frequency and expression level of $ST2^+$ Treg cells in the mouse liver (Fig. 5H-5K; Fig. S4). The expression of functional molecules, such as CTLA4, PD-1, and KLRG1 on Treg cells (*48*) was also enhanced by IL-33 (Fig. 5L; Fig. S4). Therefore, it is strongly suggested that IL-33 increased the number of $ST2^+$ Treg cells and activated Treg cell function in the liver.

Thereafter, we crossed ST2-floxed mice (*49*) and Foxp3-Cre-Yfp mice (*50*) to generate Treg-cell-specific ST2-deficient mice to exclude the possibility of the effect of ST2 on other types of cells, such as Tconv. The number of tumors was significantly reduced in $ST2^{fl/fl}$-Foxp3-Cre-Yfp mice compared to that in $ST2^{fl/fl}$-Foxp3-WT mice, while the body weights were similar between the two groups (Fig. 6A). Although the frequency of Treg cells ($Foxp3^+$) and Tconv cells ($Foxp3^-$) did not change (Fig. 6B; Fig.

S6), the expression levels of functional Treg cell markers, such as CTLA-4(*47*) and KLRG1(*48*), were significantly reduced in the Treg cells from $ST2^{fl/fl}$-Foxp3-Cre-Yfp mouse livers compared to that in $ST2^{+}$ Treg cells from the livers of $ST2^{fl/fl}$-Foxp3-WT mice (Fig. 6D; Fig. S6). Cytotoxic $CD8^{+}$ T cells in the tumor area often become dysfunctional, over-express suppressive molecules, such as PD-1, and show exhausted phenotypes with impaired proliferation and reduced cytokine production (*51*). Indeed, PD-1^{hi} $CD8^{+}$ T cells from the livers of wild-type HFD-fed mice showed a significantly lower expression of Ki-67 compared to PD-$1^{-}CD8^{+}$ T cells after anti-CD3/CD28 monoclonal antibody (mAb) stimulation (Fig. S7A-S7C). The production of effector cytokines, IFN-γ, TNF-α, and IL-2, was also impaired in PD-1^{hi} $CD8^{+}$ T cells (Fig. S7D). Interestingly, the frequency of PD-1 expressing $CD8^{+}$ T cells (PD-1^{hi} $CD8^{+}$ T) was significantly reduced in $ST2^{fl/fl}$-Foxp3-Cre-Yfp mice, although the total number of $CD8^{+}$ T cells was unchanged (Fig. 6C; Fig. S7A). These results indicate that ST2 expression in Treg cells profoundly attenuated cytotoxic $CD8^{+}$ T cell function *in vivo*. Moreover, when we injected mice with anti-ST2 blocking mAb, the number of tumors was significantly reduced (Fig. 6E), implying the therapeutic potential of the ST2 blocking antibody. These results suggest that $ST2^{+}$ Treg cells play a crucial role in the liver tumor microenvironment in promoting obesity-associated HCC development by inducing $CD8^{+}$ T cell exhaustion.

The cleaved form of GSDMD N-terminus was accumulated in HSCs in human non-viral HCC

To evaluate the relevance in humans, we first investigated the characteristics of DCA-treated senescent human HSCs in culture. The DCA-induced senescence led to the

upregulation of p16 and p21, and additional treatment with IL-1β resulted in the strong induction of SASP factors IL-33 and IL-6 (Fig. 7A). This indicates that the IL-1β-dependent IL-33 expression was conserved in human HSCs. The CELA1 induction by DCA was also confirmed in human primary HSCs (Fig. 7A).

Moreover, we examined the IL-33 expression in HSCs in human non-viral HCC tissues. Consistent with the results of the murine obesity-associated HCC model (Fig. 1 and 2), we confirmed the expression of IL-33 in the α-SMA-positive HSCs in the lipid-rich tumor regions of human non-viral HCC as we previously reported (Fig. 7B and C)(*9*), indicating that senescent HSCs in human HCC tumor region exhibit SASP phenotype, since the α-SMA-positivity in HSCs in the tumor region is well correlated with the induction of cellular senescence (Fig. 1H) (*8*). Importantly, many of the α-SMA-positive senescent HSCs were also positive for GSDMD N-terminus when stained with an antibody specifically recognizing this cleaved form of GSDMD, suggesting that GSDMD N-terminus pore was also formed in the senescent HSCs in human non-viral HCC tumor area (Fig. 7B). These results suggest that IL-33 is a SASP factor in senescent HSCs in the human non-viral liver tumor microenvironment and that a similar release mechanism of SASP factors by GSDMD N-terminus pore from HSCs could be involved in promoting the obesity-associated HCC development in humans. Our data suggest that blocking the GSDMD N-terminus pore using disulfiram, a known inhibitor of GSDMD N-terminus pore (*42*), could be a therapeutic potential.

Discussion

SASP, frequently observed in the tissue resident fibroblasts, is highly context-dependent phenotype showing both beneficial (e. g. tissue repair) and detrimental roles

(e. g. tumor progression) (*2, 8, 9*). However, the detailed molecular mechanisms, such as the release mechanism of SASP factors, that can be a molecular target for cancer therapy, and how SASP factors influence tumorigenesis in each biological context have been incompletely understood. In this study, using a mouse model of obesity-induced hepatocellular carcinoma (HCC), we identified the release mechanism of SASP factors, that include IL-1β and IL-1β-dependent cytokine IL-33, from senescent hepatic stellate cells via GSDMD N-terminus pore. Moreover, the released IL-33 acted on Treg cells expressing ST2, a receptor for IL-33, suppressing the anti-tumor immunity, thereby contributing to obesity-associated HCC progression (Fig. S8). Although we used a single mouse model of obesity-associated liver cancer, GSDMD N-terminus domain and IL-33 were present in HSCs in human NASH-associated liver cancer tissues, suggesting that the GSDMD-mediated release mechanism of IL-33 could be conserved in human. However, further studies are needed to generalize this molecular mechanism in other biological contexts both in human and mouse.

Recently, ST2-positive ILC2s stimulated by IL-33 were reported to be an anti-tumor immune mediator in the orthopedic implantation of pancreatic cancer models (*43*). In our model, however, while ST2-positive Treg cells are dominantly detected in liver tumor tissues, hepatic ILC2 constituted a very small population as previously reported (Fig. S5)(*44*), suggesting that ST2-positive Treg cells mediated the tumor-promoting effect by IL-33 in the liver via suppression of anti-tumor immunity. Indeed, the IL-33/ST2 axis has been reported to be associated with several types of human cancer promotion (*17, 52, 53*), and we confirmed the clear expression of IL-33 in HSCs in the human non-viral HCC tumor areas (Fig. 7B). Although the increase of ST2-positive Treg cells in human HCC has not been clarified yet, not only ST2-positive Treg cells

but also other types of ST2-positive immune cells are reportedly associated with tumorigenesis in humans (*17, 52-54*). These reports suggest that the upregulation of endogenous IL-33 in the tumor microenvironment itself might have a tumorigenic potential, and the blockade of the axis of IL-1β-dependent IL-33 toward ST2-positive immune cells could be a useful strategy for anticancer prevention or therapy as shown in Fig. 6E. Therefore, it should be noted that the effect of IL-33 could be altered by the function and the dominancy of target cells of IL-33 in each biological context.

The role of SASP in cancer seems varied depending on the stage of cancer, and it has been increasingly recognized to exhibit a tumor-promoting role as CAFs in the tumor microenvironment of advanced tumors (*1*). Regarding liver cancer, the early stage of precancerous hepatocytes, which were undergoing cellular senescence, were reported to secrete SASP factors for senescence-surveillance to eradicate the precancerous senescent hepatocytes (*55*), suggesting a tumor-suppressive role of SASP in the very early stage of hepatocarcinogenesis. On the other hand, another report showed that the suppression of cellular senescence in HSCs by crossing $p53^{flox/flox}$ and GFAP (Glial fibrillary acidic protein)-Cre mice exhibited subtle increase of HCC development (*56*), suggesting a tumor suppressive role of SASP in HSCs. However, GFAP was shown not to be predominantly expressed in HSCs but expressed in cholangiocytes (*57*), thereby making it difficult to conclude that senescent HSCs play a tumor suppressive role in advanced HCC tumors. Our current and previous studies clearly show that the SASP factors from senescent HSCs in advanced obesity-associated HCC tumors play a pivotal role in suppressing antitumor immunity, thereby contributing to the liver cancer progression(*8, 9, 58*), although we used a different carcinogenesis protocol. Our data strongly suggest that the HSCs in the tumor microenvironment of advanced obesity-

associated HCC act as typical CAFs to promote cancer progression.

Importantly, we elucidated one of the release mechanisms of SASP factor from senescent cells. Although the transcriptional and translational mechanisms for SASP factor induction were intensively investigated (*1*), the secretion of the translated SASP factors by senescent cells has yet to be elucidated. The gasdermins are a family of pore-forming proteins and five have been identified (GSDMA to E). Among them, GSDMD has recently been shown to create the N-terminus-mediated plasma membrane pore by the activated caspase-1 or -11, and it also induces an inflammatory lytic cell death called pyroptosis. We found that caspase-11, upregulated in LTA-stimulated senescent HSCs, cleaved GSDMD to create the GSDMD N-terminus domain. We also confirmed that the active form of IL-33, from which the chromatin binding domain (CBD) is lost, was released through the cell membrane pore formed by the GSDMD N-terminus domain in the senescent HSCs. Although the GSDMD N-terminus pore is an important release mechanism of IL-1β in living macrophages (*32*), we confirmed that IL-33 as well as IL-1β was released through the GSDMD N-terminus pore from senescent, non-immune HSCs, which is indeed a release mechanism of SASP factors from senescent cells.

Very interestingly, GSDMD N-terminus domain was also detected specifically in HSCs in human non-viral HCCs (Fig. 7B), suggesting that a similar release mechanism of SASP factors could be conserved in the HSCs in human non-viral HCC tumors. Therefore, blocking of GSDMD N-terminus pore by the repurposed use of disulfiram (*42*) could also be a therapeutic potential. We also showed that the hepatic accumulation of gut microbial component, LTA, triggered the GSDMD-mediated release of SASP factors from senescent HSCs, suggesting the importance of gut barrier function in preventing obesity-associated liver cancer. Overall, our current findings

could provide valuable new insights into the release mechanism and their fates/actions of SASP factors in the tumor microenvironment, and may facilitate the development of a prevention and therapeutic strategy for obesity-associated liver cancer, such as human NASH-associated HCC.

Materials and Methods

Study Design

The main goal of this study was to explore the release mechanism of SASP factors in the obesity-associated liver tumor microenvironment by focusing on the innate immune responses in hepatic stellate cells by LTA in the liver. The sample size of all the experiments were determined based on our previous studies and prior experiments that were sufficient for statistical analysis, and considering animal welfare, as indicated in the figure legends. All experiments were performed at least two times or more independently. The mouse experiments were performed unblinded as mice of different genotypes were identified and kept track of. The chemical treatment was designed according to the previously reported protocols as described in the materials and methods or figure legends. The measurements and counts are based on the visible positivity of the stained cells via the fluorescence microscopy and the visible liver tumors partly using Image J software (ver. 1.53) as described in the materials and methods and the figure legends.

Mice and diet

Wild-type C57BL/6 mice (CLEA Japan Inc), *Il33*$^{-/-}$ mice (C57BL6), that were created by crossing with heterozygous IL-33$^{+/-}$ mice (*26, 42*), *Il-1β*$^{-/-}$ mice (C57BL/6) (*27*), and

Treg-cell-specific ST2-deficient conditional knockout mice were used for liver carcinogenesis experiments. To generate Treg-cell-specific ST2-deficient conditional knockout mice, Foxp3-Cre-Yfp mice (*50*) were crossed with $ST2^{fl/fl}$ mice (*49*), and used for carcinogenesis experiments. The mice were maintained under specific pathogen-free conditions, on a 12-h light-dark cycle, and fed a normal diet (ND, D12450J Research Diet Inc., NJ, US or CE2, CLEA Japan) or a high-fat diet (HFD, D12492, Research Diet Inc., NJ, US) *ad libitum* (https://www.eptrading.co.jp/service/researchdiets/pdf/DIO%20Series.pdf). The age-matched male mice were used for all the liver carcinogenesis experiments because we previously confirmed that male mice develop liver cancer in much higher penetrance than female mice (*8*). Mice with more than 45 g weight at the age of 30 weeks old were used as obese mice for all experiments. The sample size used in this study was determined based on the expense of data collection, and the need to have sufficient statistical power. Randomization and blinding were not used in this study. All animal experiments were performed according to protocols approved by the Animal Care and Use Committee of the Tokyo University of Science (approval number: N16007) and the Osaka City University Graduate School of Medicine (approval number: 17206, 18079). Antibiotics and deoxycholic acid treatments in mice were performed as previously described (*8*) using a combination of four antibiotics (4Abx) containing ampicillin (1 g/L), neomycin (1 g /L), metronidazole (1 g /L), and vancomycin (500 mg/L) in drinking water at the age of 13 weeks old until euthanized at 30 weeks. Deoxycholic acid was dissolved in absolute ethanol and diluted in 66% propylene glycol to reduce the concentration of alcohol to 5%. 40 μg per g (weight) of deoxycholic acid or vehicle (control) fed three times per week using a feeding tube at the age of 13 weeks old until euthanized.

Chemically induced carcinogenesis

Male mice were used for the carcinogenesis experiments in this study. DMBA (7,12-dimethylbenz(*a*)anthracene, Sigma) treatments were performed as described previously (*8*). In brief, 50 μL of 0.5% DMBA in acetone was applied to the dorsal surface on postnatal day 4–5. The neonatal mice used for carcinogenesis experiments were shuffled from their littermates when grouping to avoid any littermate tendency. Afterwards, mother and pups were fed ND or HFD. At 4 weeks old, pups were weaned and continuously fed either ND or HFD until euthanized. The recombinant IL-33 used for injection to mice (Fig. 1G) was a commercially available short form of IL-33 and it is endotoxin-free (R&D, 3626-ML, Endotoxin Level <0.01 EU per 1 μg of the protein by the LAL method) and was dissolved in PBS. HFD-fed mice treated with DMBA at neonatal stage was intraperitoneally injected with 0.5 μg of recombinant murine IL-33 or PBS (Vehicle) twice a week at the age of 25 weeks old until 30 weeks old, according to the previously reported protocol(*59*). Elastatinal (Sigma, E0881) was dissolved in PBS. HFD-fed mice treated with DMBA at neonatal stage was intraperitoneally injected with 100 μg (per mouse with 50g weight) of Elastatinal or PBS (Vehicle) three times a week at the age of 30 weeks old until 35 weeks old. We used the lower dose than those in the previously reported protocol(*60*), and found it effective enough to suppress the cleavage of IL-33. Disulfiram (Merck, PHR1690) was dissolved in DMSO (250 mg/ml), and diluted in Corn oil to 80 times. HFD-fed mice treated with DMBA at neonatal stage was intraperitoneally injected with 0.5 mg of disulfiram or Corn oil with 1.25% DMSO (Vehicle) three times a week at the age of 30 weeks old until 35 weeks old in reference to the previously reported protocol(*61*). The anti-mouse ST2 mAb was generated in this

study. Detailed information is shown in Supplementary materials. HFD-fed mice treated with DMBA at neonatal stage was intraperitoneally injected with 150 μg of anti-mouse ST2 mAb or control rat IgG twice a week at the age of 22 weeks old until 30 weeks old. Evaluation of tumor number and size was determined by counting the number of visible tumors and measuring their size partly using Image J software (ver. 1.53). Representative data of two to three independent experiments are shown in the figures.

Isolation of primary hepatic stellate cells

Primary hepatic stellate cells were collected by a modified previously reported method (29). To avoid the stress response (30), all solutions were precooled on ice and all the subsequent manipulations were performed under ice-cold conditions before isolation. Mouse livers were perfused slowly via portal vein cannulation with 20–28 mL of liver perfusion medium (EGTA solution) (29) to flush out the blood at a rate of 4 mL/min, and then digested with 40–60 mL of liver digest medium (Enzyme Buffer Solution) containing ProE (1 mg/mL) (Merck) followed by 50–75 mL of Solution B containing Collagenase (1.3 mg/mL) (Wako) (29) at the same rate. Then, the livers were further digested with a ProE/Collagenase solution including DNase I (0.02 mg/mL) (Roche) for 30 min at 6 °C and passed through a 70-μm cell strainer (BD Biosciences). After centrifugation at 600 x g for 10 min, a Nycodenz gradient separation was performed to collect the hepatic stellate cells in the middle layer of the cell-Nycodenz solution (GBSS/A solution) (29) and overlayed GBSS/B solution (29). Detailed information on the solutions is shown in Table S2. Low-speed centrifugation (20–50 x g) was performed several times to exclude the hepatocytes. Hepatic stellate cells were remained in the supernatant and can be used for cell culture. The primary murine hepatic stellate

cells were sorted from this pre-sort cell suspension using the SH800 Cell Sorter (SONY) and used for quantitative PCR or Western blotting. The sorting strategy is shown in Fig. S2D. After two days of culture, the primary HSCs were used for LTA treatment or Lentivirus infection.

Histology and immunofluorescence analysis

Mouse liver tissues were fixed in 4% paraformaldehyde in PBS for 24 hours, progressively dehydrated through gradients of alcohol, and embedded in paraffin. Samples were sectioned on a microtome (5-μm-thick), deparaffinized in xylene, rehydrated, and then stained with hematoxylin and eosin (H&E). For antibody staining, deparaffinized and rehydrated sections were exposed to heat-induced antigen retrieval for 20 min in Retrieval Solution (Dako). After washing with PBS, the sections were incubated in blocking reagent (BioGenex) for 10 min at room temperature and incubated with primary antibodies overnight at 4 °C. After washing with PBS, the sections were incubated with secondary antibodies overnight at 4 °C. Fluorescence images were observed and photographed by using a fluorescence microscope (OLYMPUS IX71, objective lens; LUCPlanFLN 40 X, eyepiece; WHN 10 X, Filters; Blue(DAPI): Ex(nm) 330-385, Em(nm) 420: catalog no. U-MWU2, Green(Alexa488): Ex(nm) 470-495, Em(nm) 510-550: catalog no. U-MNIBA3, and Red(Alexa594): Ex(nm) 545-580, Em(nm) 610: catalog no.U-MWIY2). Immunofluorescence analysis for CELA-1 in liver tissue was performed using frozen sections. Mouse liver tissues were covered with O.C.T compound (SAKURA) and were frozen completely at -80℃. Frozen tissues were sectioned on a cryotome Cryostat (5-μm-thick) (Leica Biosystems). The tissue sections were dried at room temperature and were fixed with acetone for 10

min at -20℃. After washing with TBS, the sections were incubated in blocking reagent (BioGenex) for 10 min at room temperature and incubated with primary antibodies overnight at 4 °C. After washing with TBS, the sections were incubated with secondary antibodies for 1 hour at room temperature. Fluorescence images were observed and photographed by using an immunofluorescence microscope (OLYMPUS). The primary antibodies used for the mouse samples are shown in Table S1.

Plasmid constructions

To construct pCMV-5×Flag-short IL-33, the open reading frame (ORF) was amplified using mouse HSCs cDNA library as a template and primer pair shown in Table S1 (IL-33 Forward#1/IL-33 Reverse#1). The resulting fragments were inserted into the EcoRV and HindIII sites of pCMV-5×Flag (*62*). To construct pCMV-5×Myc-full length GSDMD and pCMV-5×Myc-N-terminal GSDMD, the ORF was amplified using mouse HSCs cDNA library as a template and primer pairs shown in Table S1 (GSDMD Forward#1/GSDMD Reverse#1 and GSDMD Forward#1/GSDMD Reverse#2, respectively). The resulting fragments were inserted into the EcoRI and SalI sites of pCMV-5×Myc (*62*). Plasmid constructions are shown in Fig. S9 in the supplementary materials. Plasmid transfection was performed using Polyethylenimine Max (Polyscience, Inc.) according to the manufacturer's protocol.

Knockdown of gene expressions by shRNA

Sigma mission shRNAs (shGSDMD #2: TRCN0000198776, shGSDMD #4: TRCN0000182401, shCASP11 #4: TRCN0000012270, shCASP11 #5: TRCN0000012271, shTLR2 #2: TRCN0000065676, shTLR2 #5: TRCN0000321317,

shIL-33 #1: TRCN0000173324, shIL-33 #2: TRCN0000173352) cloned into lentiviral shRNA plasmid pLKO.1 were used for silencing GSDMD, CASP11 or TLR2 expression. pLKO.1 shGFP(*63*) was used as a control. Lenti viral supernatant was prepared by co-transfecting HEK293T cells with VSV-G, psPax2, and pLKO.1 vectors. These virus-containing supernatants were infected with primary HSCs with 8 μg/mL polybrene (Nacalai tesque). After 24 hours, the medium was changed to a fresh culture medium containing 10 μg/mL puromycin, and cultured for 2 days.

Caspase-1 activity assay

Caspase-1 activity was measured using 10 μg total protein with the Caspase-1 Fluorometric Assay Kit (Abcam) according to the manufacturer's instructions. Briefly, HSCs were lysed, and insoluble organelles were removed by centrifugation at, 15,000 g for 10 min. The lysates were incubated for 1 hour at 37℃ with caspase-1 substrate conjugated to AFC (7-amino-4-trifluoromethyl coumarin). Cleavage of the substrate was measured using a Fluorescence microplate reader (Ex/Em=400/505 nm).

Lactate dehydrogenase (LDH) release assay

Culture supernatants were collected, and LDH activity was measured using the LDH Cytotoxicity Detection Kit (TakaraBio) according to the manufacturer's instructions. The percentage of LDH release was calculated by using the following formula: percentage of release = 100 × experimental LDH release/maximal LDH release. To determine the maximal LDH release, HSCs or THP-1 cells were treated with 1% Triton X-100.

Isolation of immune cells

Livers from mice were minced with scissors and vibrated in PBS (supplemented with 5% fetal bovine serum, 100 μg/mL $CaCl_2$, 100 μg/mL $MgCl_2$) containing 50 μg/mL Liberase TM (Roche) and 10 μg/mL DNase I (Roche) for 30 min at 37 °C. Digested tissues were further incubated for 5 min in the presence of 5 mM EDTA (Dojindo Laboratories) and passed through a 100-μm cell strainer (BD Biosciences). After centrifugation, the pellets were suspended in 30 mL of 35% Percoll in RPMI 1640 medium (wako) containing heparin and 0.03% $NaHCO_3$ (Gibco). Cell suspensions were centrifuged with no brake at 2000 rpm for 20 min at 20 °C. Red blood cells were lysed by RBC lysis buffer (BioLegend) and the remaining cells were filtered through a 70-μm cell strainer (BD Biosciences) and used for flow cytometry or cell sorting.

Flow cytometry

Using multicolor flow cytometry, the isolated immune cells were pre-incubated with unlabeled anti-CD16/32 mAb (2.4G2) (Bio X Cell) to avoid non-specific binding of antibodies to FcγR. Cells were then incubated with the antibodies for CD3ε, CD4, CD8α, CD45.2, KLRG1 (all from Biolegend), PD-1 (eBioscience), ST2 (MD Bioscience), and Neuropilin-1 (Nrp-1) (R&D Systems). Cells were fixed and permeabilized using a Foxp3 staining buffer kit (eBioscience), and then intracellularly stained for Foxp3 (eBioscience), CLTA-4 (Biolegend), and Helios (Biolegend). Detailed antibody information is shown in Table S1. Stained cells were analyzed by Attune NxT (Thermo Fisher) and data were processed by FlowJo Version 10 (FlowJo). Dead cells were excluded using Zombie NIR fixable viability dye (BioLegend).

Purification and culture of CD8 T cells and measurement of cytokine production

Immune cells from livers of DMBA-treated HFD-fed WT mice were labeled with antibodies to mouse CD8a (53-6.7, BioLegend), CD4 (RM4-4, BioLegend), and PD-1 (RMP1-30, eBioscience), and PD-1$^-$ or PD-1$^+$ CD8 T cells were sorted using FACSDiva and FACSAria II (BD Biosciences). Purified PD-1$^-$ or PD-1$^+$ CD8 T cells (0.25 × 105) were seeded with pre-coated anti-CD3ε mAb (5 μg/mL, BioLegend) and soluble anti-CD28 mAb (2.5 μg/mL BioLegend) for 3 days at 37 °C under 5% CO2 in 96-well flat-bottomed plates in a volume of 0.2 ml RPMI containing 10% FBS and 1% streptomycin plus penicillin. After incubation, the culture supernatant was collected, and cytokine concentration was measured by an Enzyme-Linked Immunosorbent Assay (ELISA) development kit for mouse tumor necrotic factor (TNF), interferon-gamma (IFN-γ), and interleukin-2 (IL-2) (eBioscience). Cultured cells were fixed, permeabilized, and stained for Ki-67 (BioLegend). Data were acquired by Attune Nxt (Thermo Fisher) and analyzed with FlowJo (Tree Star). Detailed antibody information is shown in Table S1.

Human subjects

Informed consent was obtained from patients who had surgical operations at the Osaka City University hospital according to the study protocol (no. 3722) approved by the ethics committee of the Osaka City University Graduate School of Medicine. Detailed information about the human subjects is shown in Fig. 7C and its legend.

Statistical analysis

To evaluate the normality of the data distribution, each group of data was first checked using Shapiro-Wilk test. If the *p*-value is less than 0.05, Mann-Whitney test was used. If

the *p*-value was more than 0.05, the data distribution was further evaluated using F-test for the pairwise comparisons between two samples. Student's two-tailed unpaired (two-sided) t-test (in case that *p*-value of F-test is more than 0.05) or Welch's t-test (in case that *p*-value of F-test is less than 0.05), were used. For three or more samples, one, two or three-way analysis of variance (ANOVA) with Bonferroni's multiple comparisons test was used. In all cases, the *p*-values less than 0.05 were considered significant. All the details are described in the raw data sheet in the supplementary Table S3. All statistical analyses listed here were performed using GraphPad Prism (ver. 8) software.

Other methods are shown in the Supplementary materials as below.

Materials and Methods

Fig. S1. HSCs in the tumor microenvironment of HFD-fed mice show a senescent phenotype.

Fig. S2. The markers of cellular senescence and SASP are upregulated in HSCs from HFD-induced tumor region.

Fig. S3. IL-33 deficiency does not affect the LTA-TLR2 signaling

Fig. S4. Characterization of the Treg population from the liver of DMBA-treated mice.

Fig. S5. Characterization of the ILC2 population from the liver of DMBA-treated mice.

Fig. S6. Characterization of the T cell population from the liver of ST2fl/fl-Foxp3Cre mice.

Fig. S7. Cytotoxic CD8+ T cells over-expressing PD-1 in the tumor microenvironment show exhausted phenotypes in this mouse model.

Fig. S8. Summary scheme of the present work: The release mechanism of IL-1b and IL-33 from senescent HSCs and their tumorigenic orchestration.

Fig. S9. The maps of plasmids constructed in this study.

Other Supplementary Materials for this manuscript include the followings:

Fig. S10. Full gel scans for Western blotting data.

Table S1. The list of antibodies and primers used in this study

Table S2. Reagents for isolating hepatic stellate cells from mouse livers

Table S3. Raw data for graphs and statistics

Acknowledgements

The authors thank members in the Dept. of Pathophysiology for critical feedback and experimental support. We thank the Research Support Platform of Osaka Metropolitan University Graduate School of Medicine for technical support.

Funding

This work was supported by AMED (Japan Agency for Medical Research and Development), AMED-CREST under grant number JP20gm1010009 (N.O.), AMED under grant number JP20fk0210050 (N.K.), JP19ck0106260 (N.O.), JP20cm0106401 (E.H.), JP20gm5010001 (E.H.) and Precursory Research for Embryonic Science and Technology (PRESTO) under grant number JPMJPR18H6 (S.N.) and Exploratory Research for Advanced Technology (ERATO) under grant number JPMJER1902 (S.F.). This study was also supported by the Japan Society for the Promotion of Science (JSPS) under grant number 19H04002 (N.O.), 19H03641 (N.K.), 18H02847 (S.N), 21H02963(S.N.), 20K16121 (T.K.), 20K15695 (M.T.), 20K16309 (R.Y.), and Japan Science and Technology agency (JST), the establishment of university fellowships

towards the creation of science technology innovation, under grant number JPMJFS 2138 (Y. N), as well as grants from Takeda Science Foundation (N.O. and F. K.) and Yakult Bio-Science Foundation (T.K. and N.O.) and Research Grant of the Princess Takamatsu Cancer Research Fund 18-25003 (N.O.),

Author Contributions

Conceptualization, N. O. and F. K.; Formal Analysis, F. K., T. K and R. Y.; Funding Acquisition, N. O., T. K., R. Y., N. K., E. H., and S. N.; Investigation, N.O, F. K., R. Y., M. Nakam., S. Y., T. An., T. K., M. T., Y. C. Y. N., Y. Y-M., L. T. T. T, Y. H., T. Ar., T. M. L., T. I., S. F., and S. Y.; Project Administration, N. O. and F. K.; Resources, M. Nanaj., H. A., S. M., M. K., H. T., Y. Y-M., N. K., W-Y. C., A. R., Y. I. and S. N; Supervision, N. O.; Validation, N. O, F. K and R. Y; Visualization, N. O: Writing – Original Draft Preparation, N. O. and F. K.; Writing – Review & Editing, N. O. E. H. and S. N.

Competing Interests

The authors declare no competing interests.

Data and materials availability

The Microarray analyses data are available in the GEO databases (accession number GSE151620, https://www.ncbi.nlm.nih.gov/geo/query/acc.cgi?acc=GSE151620).

All data needed to evaluate the conclusions in the paper are present in the paper or the Supplementary Materials.

References

1. V. Gorgoulis, P. D. Adams, A. Alimonti, D. C. Bennett, O. Bischof, C. Bishop, J. Campisi, M. Collado, K. Evangelou, G. Ferbeyre, J. Gil, E. Hara, V. Krizhanovsky, D. Jurk, A. B. Maier, M. Narita, L. Niedernhofer, J. F. Passos, P. D. Robbins, C. A. Schmitt, J. Sedivy, K. Vougas, T. von Zglinicki, D. Zhou, M. Serrano, M. Demaria, Cellular Senescence: Defining a Path Forward. *Cell* **179**, 813-827 (2019).
2. D. V. Faget, Q. Ren, S. A. Stewart, Unmasking senescence: context-dependent effects of SASP in cancer. *Nature reviews. Cancer* **19**, 439-453 (2019).
3. J. P. Coppe, C. K. Patil, F. Rodier, Y. Sun, D. P. Munoz, J. Goldstein, P. S. Nelson, P. Y. Desprez, J. Campisi, Senescence-associated secretory phenotypes reveal cell-nonautonomous functions of oncogenic RAS and the p53 tumor suppressor. *PLoS Biol* **6**, 2853-2868 (2008).
4. T. Kuilman, D. S. Peeper, Senescence-messaging secretome: SMS-ing cellular stress. *Nature reviews. Cancer* **9**, 81-94 (2009).
5. R. M. Laberge, Y. Sun, A. V. Orjalo, C. K. Patil, A. Freund, L. Zhou, S. C. Curran, A. R. Davalos, K. A. Wilson-Edell, S. Liu, C. Limbad, M. Demaria, P. Li, G. B. Hubbard, Y. Ikeno, M. Javors, P. Y. Desprez, C. C. Benz, P. Kapahi, P. S. Nelson, J. Campisi, MTOR regulates the pro-tumorigenic senescence-associated secretory phenotype by promoting IL1A translation. *Nature cell biology* **17**, 1049-1061 (2015).
6. T. Li, Z. J. Chen, The cGAS-cGAMP-STING pathway connects DNA damage to inflammation, senescence, and cancer. *J Exp Med* **215**, 1287-1299 (2018).
7. Q. M. Anstee, H. L. Reeves, E. Kotsiliti, O. Govaere, M. Heikenwalder, From NASH to HCC: current concepts and future challenges. *Nature reviews. Gastroenterology & hepatology* **16**, 411-428 (2019).
8. S. Yoshimoto, T. M. Loo, K. Atarashi, H. Kanda, S. Sato, S. Oyadomari, Y. Iwakura, K. Oshima, H. Morita, M. Hattori, K. Honda, Y. Ishikawa, E. Hara, N. Ohtani, Obesity-induced gut microbial metabolite promotes liver cancer through senescence secretome. *Nature* **499**, 97-101 (2013).
9. T. M. Loo, F. Kamachi, Y. Watanabe, S. Yoshimoto, H. Kanda, Y. Arai, Y. Nakajima-Takagi, A. Iwama, T. Koga, Y. Sugimoto, T. Ozawa, M. Nakamura, M. Kumagai, K. Watashi, M. M. Taketo, T. Aoki, S. Narumiya, M. Oshima, M. Arita, E. Hara, N. Ohtani, Gut Microbiota Promotes Obesity-Associated Liver Cancer through PGE2-Mediated Suppression of Antitumor Immunity. *Cancer discovery* **7**, 522-538 (2017).
10. F. Y. Liew, J. P. Girard, H. R. Turnquist, Interleukin-33 in health and disease. *Nature reviews. Immunology* **16**, 676-689 (2016).
11. M. Peine, R. M. Marek, M. Lohning, IL-33 in T Cell Differentiation, Function, and Immune Homeostasis. *Trends Immunol* **37**, 321-333 (2016).
12. C. Cayrol, J. P. Girard, Interleukin-33 (IL-33): A nuclear cytokine from the IL-1 family. *Immunological reviews* **281**, 154-168 (2018).
13. C. Cayrol, J. P. Girard, IL-33: an alarmin cytokine with crucial roles in innate immunity, inflammation and allergy. *Curr Opin Immunol* **31**, 31-37 (2014).
14. E. Lefrancais, S. Roga, V. Gautier, A. Gonzalez-de-Peredo, B. Monsarrat, J. P. Girard, C. Cayrol, IL-33 is processed into mature bioactive forms by neutrophil elastase and cathepsin G. *Proceedings of the National Academy of Sciences of the United States of America* **109**, 1673-1678 (2012).
15. E. Lefrancais, A. Duval, E. Mirey, S. Roga, E. Espinosa, C. Cayrol, J. P. Girard, Central domain of IL-33 is cleaved by mast cell proteases for potent activation of group-2 innate lymphoid cells. *Proceedings of the National Academy of Sciences of the United States of America* **111**, 15502-15507 (2014).
16. T. Ohno, H. Morita, K. Arae, K. Matsumoto, S. Nakae, Interleukin-33 in allergy. *Allergy* **67**, 1203-1214 (2012).
17. M. F. Eissmann, C. Dijkstra, A. Jarnicki, T. Phesse, J. Brunnberg, A. R. Poh, N. Etemadi, E. Tsantikos, S. Thiem, N. D. Huntington, M. L. Hibbs, A. Boussioutas, M.

A. Grimbaldeston, M. Buchert, R. J. J. O'Donoghue, F. Masson, M. Ernst, IL-33-mediated mast cell activation promotes gastric cancer through macrophage mobilization. *Nature communications* **10**, 2735 (2019).

18. A. Li, R. H. Herbst, D. Canner, J. M. Schenkel, O. C. Smith, J. Y. Kim, M. Hillman, A. Bhutkar, M. S. Cuoco, C. G. Rappazzo, P. Rogers, C. Dang, L. Jerby-Arnon, O. Rozenblatt-Rosen, L. Cong, M. Birnbaum, A. Regev, T. Jacks, IL-33 Signaling Alters Regulatory T Cell Diversity in Support of Tumor Development. *Cell Rep* **29**, 2998-3008 e2998 (2019).
19. A. H. Ameri, S. Moradi Tuchayi, A. Zaalberg, J. H. Park, K. H. Ngo, T. Li, E. Lopez, M. Colonna, R. T. Lee, M. Mino-Kenudson, S. Demehri, IL-33/regulatory T cell axis triggers the development of a tumor-promoting immune environment in chronic inflammation. *Proceedings of the National Academy of Sciences of the United States of America* **116**, 2646-2651 (2019).
20. E. Pastille, M. H. Wasmer, A. Adamczyk, V. P. Vu, L. F. Mager, N. N. T. Phuong, V. Palmieri, C. Simillion, W. Hansen, S. Kasper, M. Schuler, B. Muggli, K. D. McCoy, J. Buer, I. Zlobec, A. M. Westendorf, P. Krebs, The IL-33/ST2 pathway shapes the regulatory T cell phenotype to promote intestinal cancer. *Mucosal Immunol* **12**, 990-1003 (2019).
21. A. De Boeck, B. Y. Ahn, C. D'Mello, X. Lun, S. V. Menon, M. M. Alshehri, F. Szulzewsky, Y. Shen, L. Khan, N. H. Dang, E. Reichardt, K. A. Goring, J. King, C. J. Grisdale, N. Grinshtein, D. Hambardzumyan, K. M. Reilly, M. D. Blough, J. G. Cairncross, V. W. Yong, M. A. Marra, S. J. M. Jones, D. R. Kaplan, K. D. McCoy, E. C. Holland, P. Bose, J. A. Chan, S. M. Robbins, D. L. Senger, Glioma-derived IL-33 orchestrates an inflammatory brain tumor microenvironment that accelerates glioma progression. *Nature communications* **11**, 4997 (2020).
22. Z. Jin, L. Lei, D. Lin, Y. Liu, Y. Song, H. Gong, Y. Zhu, Y. Mei, B. Hu, Y. Wu, G. Zhang, H. Liu, IL-33 Released in the Liver Inhibits Tumor Growth via Promotion of CD4(+) and CD8(+) T Cell Responses in Hepatocellular Carcinoma. *J Immunol* **201**, 3770-3779 (2018).
23. R. Zhao, Z. Yu, M. Li, Y. Zhou, Interleukin-33/ST2 Signaling Promotes Hepatocellular Carcinoma Cell Stemness Expansion Through Activating c-Jun N-terminal Kinase Pathway. *Am J Med Sci* **358**, 279-288 (2019).
24. W. Wang, J. Wu, M. Ji, C. Wu, Exogenous interleukin-33 promotes hepatocellular carcinoma growth by remodelling the tumour microenvironment. *J Transl Med* **18**, 477 (2020).
25. P. Orning, E. Lien, K. A. Fitzgerald, Gasdermins and their role in immunity and inflammation. *J Exp Med* **216**, 2453-2465 (2019).
26. K. Oboki, T. Ohno, N. Kajiwara, K. Arae, H. Morita, A. Ishii, A. Nambu, T. Abe, H. Kiyonari, K. Matsumoto, K. Sudo, K. Okumura, H. Saito, S. Nakae, IL-33 is a crucial amplifier of innate rather than acquired immunity. *Proceedings of the National Academy of Sciences of the United States of America* **107**, 18581-18586 (2010).
27. R. Horai, M. Asano, K. Sudo, H. Kanuka, M. Suzuki, M. Nishihara, M. Takahashi, Y. Iwakura, Production of mice deficient in genes for interleukin (IL)-1alpha, IL-1beta, IL-1alpha/beta, and IL-1 receptor antagonist shows that IL-1beta is crucial in turpentine-induced fever development and glucocorticoid secretion. *J Exp Med* **187**, 1463-1475 (1998).
28. I. C. Scott, J. B. Majithiya, C. Sanden, P. Thornton, P. N. Sanders, T. Moore, M. Guscott, D. J. Corkill, J. S. Erjefalt, E. S. Cohen, Interleukin-33 is activated by allergen- and necrosis-associated proteolytic activities to regulate its alarmin activity during epithelial damage. *Sci Rep* **8**, 3363 (2018).
29. I. Mederacke, D. H. Dapito, S. Affo, H. Uchinami, R. F. Schwabe, High-yield and high-purity isolation of hepatic stellate cells from normal and fibrotic mouse livers. *Nat Protoc* **10**, 305-315 (2015).

30. M. Adam, A. S. Potter, S. S. Potter, Psychrophilic proteases dramatically reduce single-cell RNA-seq artifacts: a molecular atlas of kidney development. *Development* **144**, 3625-3632 (2017).
31. A. Freund, R. M. Laberge, M. Demaria, J. Campisi, Lamin B1 loss is a senescence-associated biomarker. *Mol Biol Cell* **23**, 2066-2075 (2012).
32. C. L. Evavold, J. Ruan, Y. Tan, S. Xia, H. Wu, J. C. Kagan, The Pore-Forming Protein Gasdermin D Regulates Interleukin-1 Secretion from Living Macrophages. *Immunity* **48**, 35-44 e36 (2018).
33. V. A. Rathinam, K. A. Fitzgerald, Inflammasome Complexes: Emerging Mechanisms and Effector Functions. *Cell* **165**, 792-800 (2016).
34. M. Ringelhan, D. Pfister, T. O'Connor, E. Pikarsky, M. Heikenwalder, The immunology of hepatocellular carcinoma. *Nature immunology* **19**, 222-232 (2018).
35. A. Ito, A. Mukaiyama, Y. Itoh, H. Nagase, I. B. Thogersen, J. J. Enghild, Y. Sasaguri, Y. Mori, Degradation of interleukin 1beta by matrix metalloproteinases. *J Biol Chem* **271**, 14657-14660 (1996).
36. A. R. Young, M. Narita, SASP reflects senescence. *EMBO Rep* **10**, 228-230 (2009).
37. U. Schonbeck, F. Mach, P. Libby, Generation of biologically active IL-1 beta by matrix metalloproteinases: a novel caspase-1-independent pathway of IL-1 beta processing. *J Immunol* **161**, 3340-3346 (1998).
38. Z. Dou, K. Ghosh, M. G. Vizioli, J. Zhu, P. Sen, K. J. Wangensteen, J. Simithy, Y. Lan, Y. Lin, Z. Zhou, B. C. Capell, C. Xu, M. Xu, J. E. Kieckhaefer, T. Jiang, M. Shoshkes-Carmel, K. Tanim, G. N. Barber, J. T. Seykora, S. E. Millar, K. H. Kaestner, B. A. Garcia, P. D. Adams, S. L. Berger, Cytoplasmic chromatin triggers inflammation in senescence and cancer. *Nature* **550**, 402-406 (2017).
39. N. Kayagaki, I. B. Stowe, B. L. Lee, K. O'Rourke, K. Anderson, S. Warming, T. Cuellar, B. Haley, M. Roose-Girma, Q. T. Phung, P. S. Liu, J. R. Lill, H. Li, J. Wu, S. Kummerfeld, J. Zhang, W. P. Lee, S. J. Snipas, G. S. Salvesen, L. X. Morris, L. Fitzgerald, Y. Zhang, E. M. Bertram, C. C. Goodnow, V. M. Dixit, Caspase-11 cleaves gasdermin D for non-canonical inflammasome signalling. *Nature* **526**, 666-671 (2015).
40. J. Shi, Y. Zhao, K. Wang, X. Shi, Y. Wang, H. Huang, Y. Zhuang, T. Cai, F. Wang, F. Shao, Cleavage of GSDMD by inflammatory caspases determines pyroptotic cell death. *Nature* **526**, 660-665 (2015).
41. P. Broz, P. Pelegrin, F. Shao, The gasdermins, a protein family executing cell death and inflammation. *Nature reviews. Immunology* **20**, 143-157 (2020).
42. J. J. Hu, X. Liu, S. Xia, Z. Zhang, Y. Zhang, J. Zhao, J. Ruan, X. Luo, X. Lou, Y. Bai, J. Wang, L. R. Hollingsworth, V. G. Magupalli, L. Zhao, H. R. Luo, J. Kim, J. Lieberman, H. Wu, FDA-approved disulfiram inhibits pyroptosis by blocking gasdermin D pore formation. *Nature immunology* **21**, 736-745 (2020).
43. J. A. Moral, J. Leung, L. A. Rojas, J. Ruan, J. Zhao, Z. Sethna, A. Ramnarain, B. Gasmi, M. Gururajan, D. Redmond, G. Askan, U. Bhanot, E. Elyada, Y. Park, D. A. Tuveson, M. Gonen, S. D. Leach, J. D. Wolchok, R. P. DeMatteo, T. Merghoub, V. P. Balachandran, ILC2s amplify PD-1 blockade by activating tissue-specific cancer immunity. *Nature* **579**, 130-135 (2020).
44. S. Steinmann, M. Schoedsack, F. Heinrich, P. C. Breda, A. Ochel, G. Tiegs, K. Neumann, Hepatic ILC2 activity is regulated by liver inflammation-induced cytokines and effector CD4(+) T cells. *Sci Rep* **10**, 1071 (2020).
45. S. Sakaguchi, D. A. Vignali, A. Y. Rudensky, R. E. Niec, H. Waldmann, The plasticity and stability of regulatory T cells. *Nature reviews. Immunology* **13**, 461-467 (2013).
46. N. Ohkura, Y. Kitagawa, S. Sakaguchi, Development and maintenance of regulatory T cells. *Immunity* **38**, 414-423 (2013).
47. K. Wing, Y. Onishi, P. Prieto-Martin, T. Yamaguchi, M. Miyara, Z. Fehervari, T. Nomura, S. Sakaguchi, CTLA-4 control over Foxp3+ regulatory T cell function.

Science **322**, 271-275 (2008).
48. A. Vasanthakumar, K. Moro, A. Xin, Y. Liao, R. Gloury, S. Kawamoto, S. Fagarasan, L. A. Mielke, S. Afshar-Sterle, S. L. Masters, S. Nakae, H. Saito, J. M. Wentworth, P. Li, W. Liao, W. J. Leonard, G. K. Smyth, W. Shi, S. L. Nutt, S. Koyasu, A. Kallies, The transcriptional regulators IRF4, BATF and IL-33 orchestrate development and maintenance of adipose tissue-resident regulatory T cells. *Nature immunology* **16**, 276-285 (2015).
49. W. Y. Chen, J. Hong, J. Gannon, R. Kakkar, R. T. Lee, Myocardial pressure overload induces systemic inflammation through endothelial cell IL-33. *Proceedings of the National Academy of Sciences of the United States of America* **112**, 7249-7254 (2015).
50. Y. P. Rubtsov, J. P. Rasmussen, E. Y. Chi, J. Fontenot, L. Castelli, X. Ye, P. Treuting, L. Siewe, A. Roers, W. R. Henderson, Jr., W. Muller, A. Y. Rudensky, Regulatory T cell-derived interleukin-10 limits inflammation at environmental interfaces. *Immunity* **28**, 546-558 (2008).
51. D. M. Pardoll, The blockade of immune checkpoints in cancer immunotherapy. *Nature reviews. Cancer* **12**, 252-264 (2012).
52. Y. H. Wen, H. Q. Lin, H. Li, Y. Zhao, V. W. Y. Lui, L. Chen, X. M. Wu, W. Sun, W. P. Wen, Stromal interleukin-33 promotes regulatory T cell-mediated immunosuppression in head and neck squamous cell carcinoma and correlates with poor prognosis. *Cancer Immunol Immunother* **68**, 221-232 (2019).
53. S. Taniguchi, A. Elhance, A. Van Duzer, S. Kumar, J. J. Leitenberger, N. Oshimori, Tumor-initiating cells establish an IL-33-TGF-beta niche signaling loop to promote cancer progression. *Science* **369**, (2020).
54. G. Ercolano, A. Gomez-Cadena, N. Dumauthioz, G. Vanoni, M. Kreutzfeldt, T. Wyss, L. Michalik, R. Loyon, A. Ianaro, P. C. Ho, C. Borg, M. Kopf, D. Merkler, P. Krebs, P. Romero, S. Trabanelli, C. Jandus, PPAR drives IL-33-dependent ILC2 pro-tumoral functions. *Nature communications* **12**, 2538 (2021).
55. T. W. Kang, T. Yevsa, N. Woller, L. Hoenicke, T. Wuestefeld, D. Dauch, A. Hohmeyer, M. Gereke, R. Rudalska, A. Potapova, M. Iken, M. Vucur, S. Weiss, M. Heikenwalder, S. Khan, J. Gil, D. Bruder, M. Manns, P. Schirmacher, F. Tacke, M. Ott, T. Luedde, T. Longerich, S. Kubicka, L. Zender, Senescence surveillance of pre-malignant hepatocytes limits liver cancer development. *Nature* **479**, 547-551 (2011).
56. A. Lujambio, L. Akkari, J. Simon, D. Grace, D. F. Tschaharganeh, J. E. Bolden, Z. Zhao, V. Thapar, J. A. Joyce, V. Krizhanovsky, S. W. Lowe, Non-cell-autonomous tumor suppression by p53. *Cell* **153**, 449-460 (2013).
57. I. Mederacke, C. C. Hsu, J. S. Troeger, P. Huebener, X. Mu, D. H. Dapito, J. P. Pradere, R. F. Schwabe, Fate tracing reveals hepatic stellate cells as dominant contributors to liver fibrosis independent of its aetiology. *Nature communications* **4**, 2823 (2013).
58. A. Takahashi, T. M. Loo, R. Okada, F. Kamachi, Y. Watanabe, M. Wakita, S. Watanabe, S. Kawamoto, K. Miyata, G. N. Barber, N. Ohtani, E. Hara, Downregulation of cytoplasmic DNases is implicated in cytoplasmic DNA accumulation and SASP in senescent cells. *Nature communications* **9**, 1249 (2018).
59. J. R. Brestoff, B. S. Kim, S. A. Saenz, R. R. Stine, L. A. Monticelli, G. F. Sonnenberg, J. J. Thome, D. L. Farber, K. Lutfy, P. Seale, D. Artis, Group 2 innate lymphoid cells promote beiging of white adipose tissue and limit obesity. *Nature* **519**, 242-246 (2015).
60. K. K. Bali, R. Kuner, Therapeutic potential for leukocyte elastase in chronic pain states harboring a neuropathic component. *Pain* **158**, 2243-2258 (2017).
61. M. Bernier, S. J. Mitchell, D. Wahl, A. Diaz, A. Singh, W. Seo, M. Wang, A. Ali, T. Kaiser, N. L. Price, M. A. Aon, E. Y. Kim, M. A. Petr, H. Cai, A. Warren, C. Di Germanio, A. Di Francesco, K. Fishbein, V. Guiterrez, D. Harney, Y. C. Koay, J. Mach, I. N. Enamorado, T. Pulpitel, Y. Wang, J. Zhang, L. Zhang, R. G. Spencer, K.

G. Becker, J. M. Egan, E. G. Lakatta, J. O'Sullivan, M. Larance, D. G. LeCouteur, V. C. Cogger, B. Gao, C. Fernandez-Hernando, A. M. Cuervo, R. de Cabo, Disulfiram Treatment Normalizes Body Weight in Obese Mice. *Cell Metab* **32**, 203-214 e204 (2020).
62. L. Ruan, M. Osawa, N. Hosoda, S. Imai, A. Machiyama, T. Katada, S. Hoshino, I. Shimada, Quantitative characterization of Tob interactions provides the thermodynamic basis for translation termination-coupled deadenylase regulation. *J Biol Chem* **285**, 27624-27631 (2010).
63. Y. Sancak, T. R. Peterson, Y. D. Shaul, R. A. Lindquist, C. C. Thoreen, L. Bar-Peled, D. M. Sabatini, The Rag GTPases bind raptor and mediate amino acid signaling to mTORC1. *Science* **320**, 1496-1501 (2008).

Figure legends

Fig. 1. IL-33 promotes obesity-associated HCC development.

A, Log2-fold changes of cytokine gene expression level of the tumor region compared to that of the non-tumor region of DMBA-treated HFD-fed WT mouse livers (n = 3, from microarray analysis data). DMBA; 7,12-dimethylbenz[a]anthracen, HFD; high-fat diet, WT; wild-type. **B,** Heat map representation of the cytokine gene expression level of non-tumor region and tumor regions of DMBA-treated HFD-fed WT mouse livers (n = 3) (from microarray analysis data). The heat map key indicates log2-fold changes from the average data (n = 2) of normal diet-fed mouse livers as a baseline. **C,** qPCR analysis of *Il33* gene expression in DMBA-treated HFD-fed WT mouse livers (n = 6). NT; non-tumor region of HFD-fed mice. T; tumor region of HFD-fed mice. **D,** Liver tissue lysates from DMBA-treated HFD-fed WT mice or DMBA-treated HFD-fed $Il33^{-/-}$ mice were subjected to immune blotting using anti-IL-33 antibody (lysates from representative two mice from each group). β-actin was used as a loading control. **E,** Timeline of the experimental procedure shown in panel F and G. Eut means euthanasia. **F,** i) The total liver tumor number at the age of 30 weeks. ii) Representative macroscopic photograph of livers. Arrowheads indicate HCCs. iii) The average liver tumor numbers and the relative size distribution at the age of 30 weeks (classified as > 6 mm, 2−6 mm, ≤ 2 mm). iv) The average body weight of each group by paired feeding. WT, n = 4; $Il33^{-/-}$, n = 7. **G,** DMBA-treated HFD-fed wild-type mice were intraperitoneally injected with 0.5 μg of recombinant murine IL-33 in PBS (rIL-33, n = 11) or PBS (Veh, n = 11) twice a week at the age of 25 weeks old until 30 weeks old. i) The total liver tumor number at the age of 30 weeks. ii) Representative macroscopic photograph of livers. Arrowheads indicate hepatocellular carcinomas (HCCs). iii) The

average liver tumor numbers and the relative size distribution at the age of 30 weeks (classified as > 6 mm, 2−6 mm, ≤ 2 mm). iv) The average body weight of each group. **H**, Immunofluorescence analysis of liver section from WT mice or *Il33*$^{-/-}$ mice kept with HFD. hepatic stellate cells (HSCs) were visualized by α-smooth muscle actin (SMA) staining (green) and the cell nuclei were stained by 4,6-diamidino-2-phenylindole (DAPI; blue). Arrowheads indicate α-SMA expressing cells that were positive for indicated markers (red). The histograms indicate the percentages of α-SMA-expressing cells that were positive for IL-33, p21 or 53BP1, and the percentages of Ki-67-expressing cells in α-SMA^{-} cells or α-SMA^{+} cells. Scale bars, 50 μm. T; tumor cell. HSC; hepatic stellate cell. Data of three mice in each group are represented and at least 100 cells were counted per group for statistical analysis. All graphs represent mean ± SEM. The indicated *p*-values were calculated by Mann Whitney test (C), Student's two-tailed unpaired *t*-test (F and G), Welch's t-test (H IL-33/α-SMA and p21/α-SMA) or two-way ANOVA with Bonferroni's multiple comparisons test (H Ki-67/α-SMA).

Fig. 2. DCA and IL-1β cooperatively induce IL-33 expression in HSCs.

A, Immunofluorescence analysis of liver section from untreated (HFD, high-fat diet-fed)(i and v), four antibiotics-treated and vehicle-treated (HFD+4Abx+Veh)(ii and vi), four antibiotics-treated and deoxycholic acid (DCA)-treated (HFD+4Abx+DCA)(iii and vii) WT mice, or *Il1b*$^{-/-}$ mice (iv and viii). HSCs were visualized by α-smooth muscle actin (SMA) staining (green) and the cell nuclei were stained by 4,6-diamidino-2-phenylindole (DAPI; blue). Upper panel; arrowheads indicate α-SMA expressing cells that were positive for IL-33 (red). Scale bars, 50 μm. Lower panel; arrowheads indicate α-SMA expressing cells that were positive for 53BP1 (red). Scale bars, 100 μm. The experiments are performed using WT mice (HFD, n = 11, HFD+4Abx+Veh, n = 3, and HFD+4Abx+DCA, n = 3) or *Il1b*$^{-/-}$ mice (n = 9) as previously described[14], and the representative immunofluorescence photographs are shown. **B, C,** The histograms indicate the percentages of IL-33-positive cells **(B)** and 53BP1-positive cells **(C)** among α-SMA-expressing cells. Data of three mice in each group are represented and at least 100 cells were counted per group for statistical analysis. **D,** Murine primary HSCs were treated with DCA for 7 days and then with IL-1β (0, 0.01, 0.1, and 1 ng/mL). After 24 hours, the cells were subjected to qPCR analysis for *Cdkn2a* (p16), *Cdkn1a* (p21),

Cxcl1 or *Il33* gene expression. All graphs represent mean ± SEM. The indicated *p* values were calculated by Mann Whitney test (B and C, WT vs IL-1β$^{-/-}$) or one-way ANOVA with Bonferroni's multiple comparisons test (B and C, WT only). The two-way ANOVA with Bonferroni's multiple comparisons test was used for (D).

Fig. 3. IL-33 is cleaved and activated by elastase CELA1.

A, Log2-fold changes of protease gene expression level of the tumor region compared to that of the non-tumor region of DMBA-treated HFD-fed WT mouse livers (n = 3, from microarray analysis data). DMBA; 7,12-dimethylbenz[a]anthracen, HFD; high-fat diet, WT; wild-type. **B,** Heat map representation of the protease gene expression level of non-tumor region and tumor regions of DMBA-treated HFD-fed WT mouse livers (n = 3) (from microarray analysis data). The heat map key indicates log2-fold changes normalized by the average data (n = 2) of normal diet-fed mouse livers as a baseline. **C,** qPCR analysis of *Cela1* gene in WT mouse livers (n = 6). NT; non-tumor region of HFD-fed mice. T; tumor regions of HFD-fed mice. **D,** Liver tissue lysates from DMBA-treated HFD-fed WT mouse were subjected to western blotting using anti-Cela1 antibody (lysates of representative two mice from each group). β-actin was used as a loading control. **E,** Immunofluorescence analysis of liver section. hepatic stellate cells (HSCs) were visualized by α-smooth muscle actin (SMA) staining (green) and the cell nuclei were stained by 4,6-diamidino-2-phenylindole (DAPI blue). Arrowheads indicate α-SMA expressing cells that were positive for CELA1 (red). The histogram indicates the percentages of α-SMA-expressing cells that were positive for CELA1. Scale bars, 50 μm. Data of three (HFD-fed) mice in each group are represented and at least 100 cells were counted per group for statistical analysis. **F,** Recombinant full-length of IL-33 was incubated with CELA1 for 15 min in the presence or absence of an elastase inhibitor (10 μM Elastatinal) and subjected to western blotting using anti-IL-33 antibody. **G,** Murine primary HSCs were treated with DCA for 7 days and then IL-1β (0, 0.01, 0.1, 1 ng/mL) was added. After 24 hours, the cells were subjected to qPCR analysis for *Cela1* gene expression. **H,** Timeline of the experimental procedure shown in panel I and J. Eut means euthanasia. DMBA-treated HFD-fed mice were intraperitoneally injected with 100 μg Elastatinal three times a week at the age of 30 weeks old until euthanized at 35 weeks old. Elastatinal, n = 7 or PBS (Veh), n = 7. **I,**

Liver tissue lysates were subjected to western blotting using anti-IL-33 antibody (n = 2). β-actin was used as a loading control. **J,** i) Representative macroscopic photograph of livers. Arrowheads indicate HCCs. ii) The total liver tumor number at the age of 35 weeks. The average liver tumor numbers and the relative size distribution at the age of 35 weeks (classified as > 6 mm, 2−6 mm, ≤ 2 mm). iii)The average body weight of mice. All graphs represent mean ± SEM. The indicated *p*-values were calculated by Mann Whitney test (C, E, and J) or two-way ANOVA with Bonferroni's multiple comparisons test (G).

Fig. 4. Short form of IL-33 is released through GSDMD N-terminus pore.

Murine primary hepatic stellate cells (HSCs) were isolated from 7,12-dimethylbenz[a]anthracene (DMBA)-treated normal diet (ND) or high-fat diet (HFD)-fed mouse livers as described in the method section. **A,** Cell lysates from freshly isolated HSCs were subjected to western blotting using antibodies shown on the left. **B,** Freshly isolated murine primary HSCs from ND-fed liver or HFD-induced liver tumor were incubated with 25μg/ml lipoteichoic acid (LTA) for 24 hours and then the cell lysates or culture supernatant were subjected to western blotting using antibodies shown on the left. **C,** Immunohistochemical staining of LTA (red) in the liver sections of DMBA-treated ND-fed wild-type (WT) mice and HFD-fed WT mice with or without four antibiotics (4Abx) treatment containing ampicillin (1 g/L), neomycin (1 g /L), metronidazole (1 g /L), and vancomycin (500 mg/L) in drinking water, or the liver sections of DMBA-treated HFD-fed *Il33*$^{-/-}$ mice. Scale bars, 50 μm. The histogram indicates the area of LTA in liver sections measured with image J software (ver. 1.53). All graphs represent mean ± SEM. The indicated *p* values were calculated by Student's two-tailed unpaired *t* test. **F, G and I,** Freshly isolated murine primary HSCs from tumor region were infected with shRNA vectors targeting GSDMD (F), caspase-11 (G), TLR2 (I) or with control shRNA vector for 2 days, and then 25μg/ml LTA was added. After 24 hours, the cell extracts or culture supernatant were subjected to immunoblotting using antibodies shown on the left. Representative data of two to three independent experiments are shown (B, E, F, G, H and I). **F,** HEK293T were co-transfected with expression vectors of Flag-tagged short IL-33 or empty vector together

with Myc-tagged N-terminal GSDMD, full length GSDMD or empty vector. After 24 hours, the cell extracts and culture supernatant were subjected to immunoblotting using antibodies shown on the left. **H,** Caspase-1 activity assay in HSCs isolated from ND-fed liver and HFD-induced liver tumor with or without LTA treatment (n = 3). **J,** Lactate dehydrogenase (LDH) release assay in THP-1 cells (H) and HSCs isolated from HFD-induced liver tumor (I). The amount of LDH released from indicate cells were measured at 1, 3, and 5 days after LTA addition (n = 3). **K,** i) Timeline of the experimental procedure. DMBA-treated HFD-fed mice were intraperitoneally injected with 500 μg disulfiram three times a week at the age of 30 weeks old until euthanized at 35 weeks old. Disulfiram, n = 7 or Corn oil (Veh), n = 4. Eut means euthanasia. ii) Representative macroscopic photograph of livers. Arrowheads indicate HCCs. iii) The total liver tumor number at the age of 35 weeks old. iv) The average liver tumor numbers and the relative size distribution at the age of 35 weeks old (classified as > 6 mm, 2−6 mm, ≤ 2 mm). v) The average body weight of mice. All graphs represent mean ± SEM. The indicated *p*-values were calculated by one-way ANOVA with Bonferroni's multiple comparisons test (C, WT only and D), two-way ANOVA with Bonferroni's multiple comparisons test (H), three-way ANOVA with Bonferroni's multiple comparisons test (J), Welch's t-test (C, WT vs Il33$^{-/-}$), or Student's two-tailed unpaired t test (K).

Fig. 5. IL-33 activates Treg cells in the liver.

A, Representative histograms of ST2 expression on hepatic stellate cells (HSCs) stimulated with deoxycholic acid (DCA)/IL-1β, primary hepatocytes from normal-diet (ND)-fed or high-fat diet (HFD)-fed wild-type (WT) mouse livers and Hepa1-6 cells. Blue line, isotype control mAb; Red line, anti-ST2 mAb.

B to G, Flow cytometric analysis of lymphocytes from livers of ND-fed (n = 5) or HFD-fed (n = 7) WT mice. Cell surface ST2 and intracellular Foxp3 expression in CD3ε$^+$CD4$^+$ cells **(B)**. Frequency of Foxp3$^+$ (Treg) or Foxp3$^-$ (Tconv) among CD3ε$^+$CD4$^+$ cells **(C)**. Frequency of ST2$^+$Foxp3$^+$ (Treg) or ST2$^+$Foxp3$^-$ (Tconv) among CD3ε$^+$CD4$^+$ cells **(D)**. Cell surface ST2 expression and neuropillin-1 (Nrp-1) **(E)** or intracellular Helios expression **(F)** in CD3ε$^+$CD4$^+$Foxp3$^+$ cells. Mean fluorescence intensity (MFI) of Foxp3, CTLA-4, PD-1 and frequency of KLRG1$^+$ in ST2$^-$

$CD3\varepsilon^+CD4^+Foxp3^+$ cells ($ST2^-$) or in $ST2^+CD3\varepsilon^+CD4^+Foxp3^+$ cells ($ST2^+$) **(G)**. **H to L,** HFD-fed WT mice were intraperitoneally injected with 0.5 μg of recombinant murine IL-33 in PBS (n = 8) or PBS (n = 8) on days 0, 2, 4 and 6, and lymphocytes from livers were analysed by flow cytometry on day 8 after the first IL-33 injection. Cell surface ST2 and intracellular Foxp3 expression in $CD3\varepsilon^+CD4^+$ cells **(H)**. Frequency of $ST2^+$ (left) and MFI of ST2 (right) in $CD3\varepsilon^+CD4^+Foxp3^+$ cells **(I)**. Frequency of $ST2^-$ $CD3\varepsilon^+CD4^+Foxp3^+$ cells ($ST2^-$ Treg) or $ST2^+CD3\varepsilon^+CD4^+Foxp3^+$ cells ($ST2^+$ Treg) among $CD3\varepsilon^+CD4^+$ cells **(J)**. Frequency of $ST2^+Foxp3^+$ (Treg) or $ST2^+Foxp3^-$ (Tconv) among $CD3\varepsilon^+CD4^+$ cells **(K)**. MFI of Foxp3, CTLA-4, PD-1 and frequency of $KLRG1^+$ in $ST2^-CD3\varepsilon^+CD4^+Foxp3^+$ cells ($ST2^-$ Treg) or in $ST2^+CD3\varepsilon^+CD4^+Foxp3^+$ cells ($ST2^+$ Treg) **(L)**. All graphs represent mean ± SEM. The indicated *p*-values were calculated by Student's two-tailed unpaired t-test (G Foxp3 and CTLA-4, and I), Welch's t-test (G PD-1 and KLRG-1), or two-way ANOVA with Bonferroni's multiple comparisons test (C, D, J, K, and L).

Fig. 6. ST2 expressing Tregs promote obesity-associated HCC development.

A to D, The livers of *ST2*$^{fl/fl}$-*Foxp3*^{WT} (n = 8) and *ST2*$^{fl/fl}$-*Foxp3*^{Cre} (n = 13) mice kept with high-fat diet (HFD) for 35 weeks after the administration of 7,12-dimethylbenz[a]anthracene (DMBA) were subjected to assays as described below. i) Representative macroscopic photograph of livers. Arrowheads indicate hepatocellular carcinomas (HCCs). ii) The total liver tumor number at the age of 35 weeks. iii) The average liver tumor numbers and the relative size distribution at the age of 35 weeks (classified as > 6 mm, 2−6 mm, ≤ 2 mm). iv) the average body weight of each group **(A)**. Frequency of $CD4^+Foxp3^+$ (left) or $CD4^+Foxp3^-$ (right) among $CD3\varepsilon^+$ cells were analyzed by flow cytometric analysis **(B)**. Frequency of $CD8^+$ among $CD3^+$ cells (left) and $PD\text{-}1^+$ among $CD3\varepsilon^+CD8^+$ cells (right) **(C)**. MFI of Foxp3, CTLA-4, PD-1 and frequency of $KLRG1^+$ in $ST2^-CD3\varepsilon^+CD4^+Foxp3^+$ cells ($ST2^-$) or in $ST2^+CD3\varepsilon^+CD4^+Foxp3^+$ cells ($ST2^+$) from *ST2*$^{fl/fl}$-*Foxp3*^{WT} mouse livers (n = 8), or $CD3\varepsilon^+CD4^+Foxp3^+$ cells from *ST2*$^{fl/fl}$-*Foxp3*^{Cre} mouse livers (n = 5) **(D)**. **E,** i) Timeline of the experimental procedure. Eut means euthanasia. DMBA-treated HFD-fed mice were intraperitoneally injected with 150 μg of anti-ST2 mAb (Anti-ST2, n = 5) or control rat IgG (Ctrl Ab, n = 6) twice a week at the age of 22 weeks old until euthanized

(30 weeks old). ii) Representative macroscopic photograph of livers. Arrowheads indicate HCCs. iii) The total liver tumor number at the age of 30 weeks. iv) The average liver tumor numbers and the relative size distribution at the age of 30 weeks (classified as > 6 mm, 2−6 mm, ≤ 2 mm). v) The average body weight of each group. All graphs represent mean ± SEM. The indicated *p*- values were calculated by Student's two-tailed unpaired t-test (A, B $FOXP3^+$, C, CD8), Welch's t-test (C PD-1), two-way ANOVA with Bonferroni's multiple comparisons test (D) or Mann Whitney test (B $FOXP3^-$, E).

Fig. 7. IL-33 and N-terminus of GSDMD are detected in HSCs in advanced non-viral HCCs in human.

A, Human primary hepatic stellate cells (HSCs) were treated with deoxycholic acid (DCA) for 15 days to induce cellular senescence and then with IL-1β (0, 0.01, 0.1, 1 ng/mL). After 6 hours, the cells were subjected to qPCR analysis for *p21, p16, IL6*, *IL33* or *CELA1* gene expression. **B,** Histology and immunofluorescence analysis of human HCC tumor regions. Paraffin embedded liver tissues from the patients of non-viral hepatocellular carcinomas (HCCs) resected in the Osaka City University hospital were examined. We previously reported that SASP secretome from senescent hepatic stellate cells was predominantly observed in non-cirrhotic HCC with high lipid accumulation in the tumor region[15]. Therefore, we focused on non-viral HCC with this feature. The histologies were examined using tumor tissues obtained from May of 2017 until April of 2018. The total number of available non-viral HCCs were n = 12 during this period. The number of non-cirrhotic HCCs with high lipid accumulation were n = 3, and the histologies of these three are shown. Upper panel; H&E staining representative images. Lower panel; HSCs were visualized by α-SMA staining (green) and the cell nuclei were stained by 4,6-diamidino-2-phenylindole (DAPI; blue). Arrowheads indicate α-SMA expressing cells that were positive for indicated markers (red). The histograms indicate the percentages of IL-33, Ki-67-expressing or N-terminal GSDMD cells in $\alpha\text{-SMA}^-$ cells or $\alpha\text{-SMA}^+$ cells. Scale bars, 100 μm. **C,** Brief information of these three patients is summarized in the table. All graphs represent mean ± SEM. The indicated *p*-values were calculated by two-way ANOVA with Bonferroni's multiple comparisons test (A) or by Mann Whitney test (B).

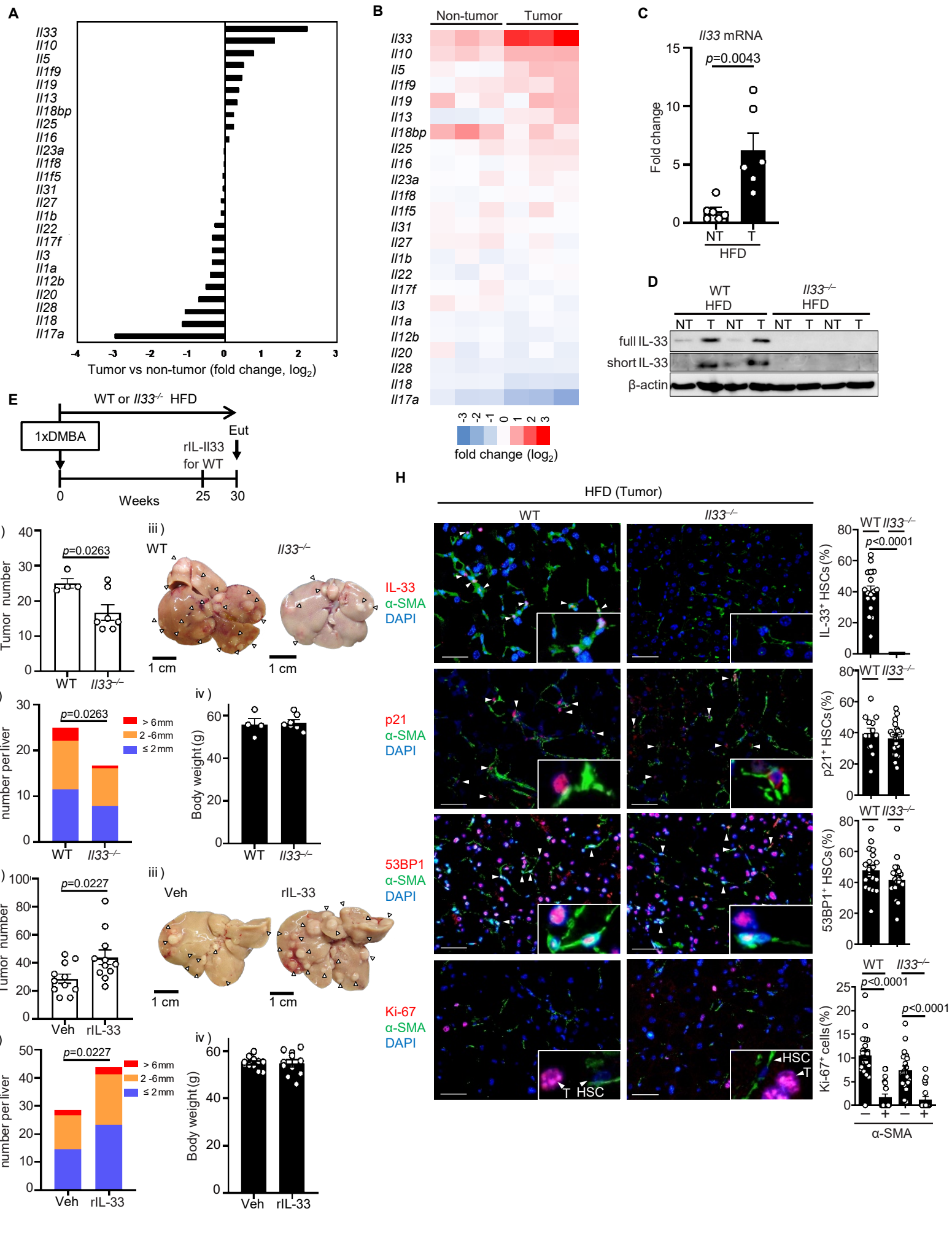
A
Il33
Il10
Il5
Il1f9
Il19
Il13
Il18bp
Il25
Il16
Il23a
Il1f8
Il1f5
Il31
Il27
Il1b
Il22
Il17f
Il3
Il1a
Il12b
Il20
Il28
Il18
Il17a
Tumor vs non-tumor (fold change, log2)
B
Non-tumor
Tumor
fold change (log2)
C
Il33 mRNA
p=0.0043
Fold change
NT
T
HFD
D
WT HFD
Il33−/− HFD
full IL-33
short IL-33
β-actin
E
WT or Il33−/− HFD
1xDMBA
Eut
rIL-Il33 for WT
Weeks
F
Tumor number
p=0.0263
Average tumor number per liver
> 6mm
2 -6mm
≤ 2mm
Body weight (g)
1 cm
G
p=0.0227
Veh
rIL-33
H
HFD (Tumor)
IL-33 α-SMA DAPI
p21 α-SMA DAPI
53BP1 α-SMA DAPI
Ki-67 α-SMA DAPI
IL-33+ HSCs (%)
p21+ HSCs (%)
53BP1+ HSCs (%)
Ki-67+ cells (%)
p<0.0001
HSC
T
α-SMA

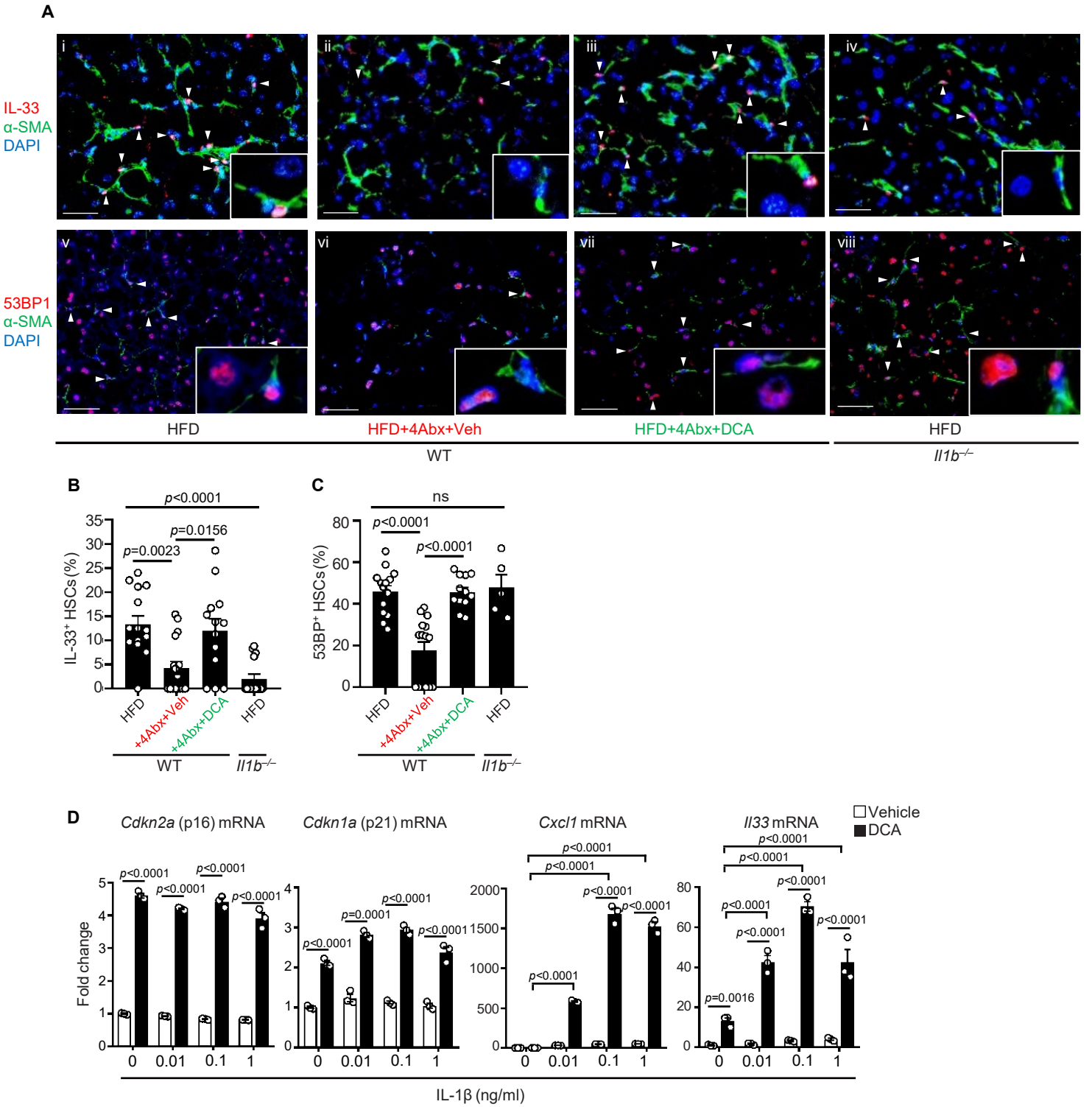
A
IL-33
α-SMA
DAPI
53BP1
α-SMA
DAPI
i
ii
iii
iv
v
vi
vii
viii
HFD
HFD+4Abx+Veh
HFD+4Abx+DCA
HFD
WT
Il1b−/−
B
IL-33+ HSCs (%)
p<0.0001
p=0.0156
p=0.0023
HFD
+4Abx+Veh
+4Abx+DCA
HFD
WT
Il1b−/−
C
53BP+ HSCs (%)
ns
p<0.0001
p<0.0001
HFD
+4Abx+Veh
+4Abx+DCA
HFD
WT
Il1b−/−
D
Cdkn2a (p16) mRNA
Cdkn1a (p21) mRNA
Cxcl1 mRNA
Il33 mRNA
Vehicle
DCA
Fold change
IL-1β (ng/ml)
0
0.01
0.1
1
p<0.0001
p=0.0016
p=0.0001

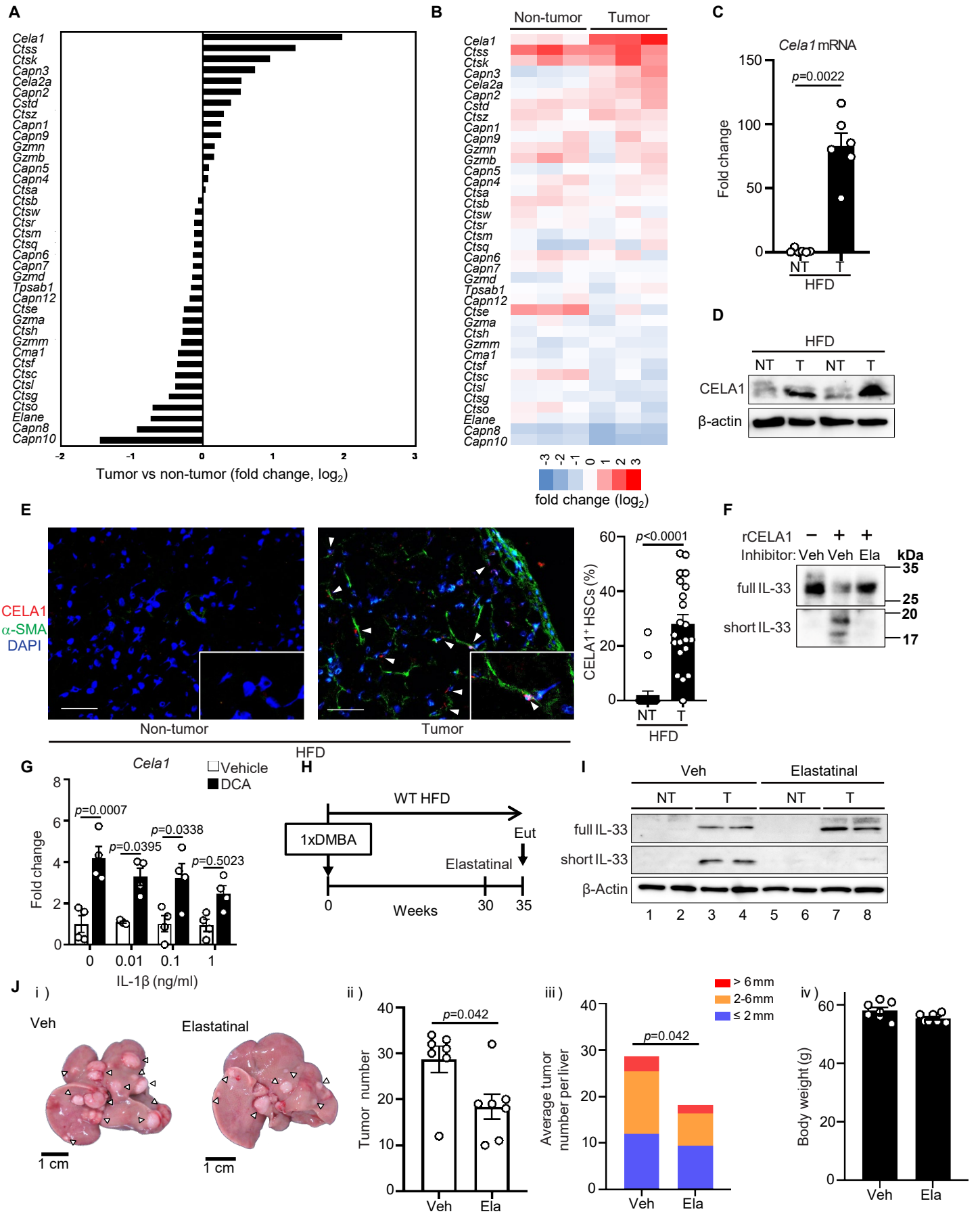
A
Cela1
Ctss
Ctsk
Capn3
Cela2a
Capn2
Cstd
Ctsz
Capn1
Capn9
Gzmn
Gzmb
Capn5
Capn4
Ctsa
Ctsb
Ctsw
Ctsr
Ctsm
Ctsq
Capn6
Capn7
Gzmd
Tpsab1
Capn12
Ctse
Gzma
Ctsh
Gzmm
Cma1
Ctsf
Ctsc
Ctsl
Ctsg
Ctso
Elane
Capn8
Capn10
-2
-1
0
1
2
3
Tumor vs non-tumor (fold change, log2)
B
Non-tumor
Tumor
-3 -2 -1 0 1 2 3
fold change (log2)
C
Cela1 mRNA
p=0.0022
Fold change
150
100
50
0
NT
T
HFD
D
HFD
NT T NT T
CELA1
β-actin
E
CELA1
α-SMA
DAPI
Non-tumor
Tumor
p<0.0001
CELA1+ HSCs (%)
60
40
20
0
NT
T
HFD
F
rCELA1 − + +
Inhibitor: Veh Veh Ela
kDa
full IL-33
short IL-33
35
25
20
17
G
Cela1
Vehicle
DCA
p=0.0007
p=0.0395
p=0.0338
p=0.5023
Fold change
8
6
4
2
0
0
0.01
0.1
1
IL-1β (ng/ml)
H
HFD
WT HFD
1xDMBA
Eut
Elastatinal
0
Weeks
30
35
I
Veh
Elastatinal
NT T NT T
full IL-33
short IL-33
β-Actin
1 2 3 4 5 6 7 8
J
i)
Veh
Elastatinal
1 cm
1 cm
ii)
p=0.042
Tumor number
40
30
20
10
0
Veh
Ela
iii)
> 6 mm
2-6 mm
≤ 2 mm
p=0.042
Average tumor number per liver
40
30
20
10
0
Veh
Ela
iv)
Body weight (g)
60
40
20
0
Veh
Ela

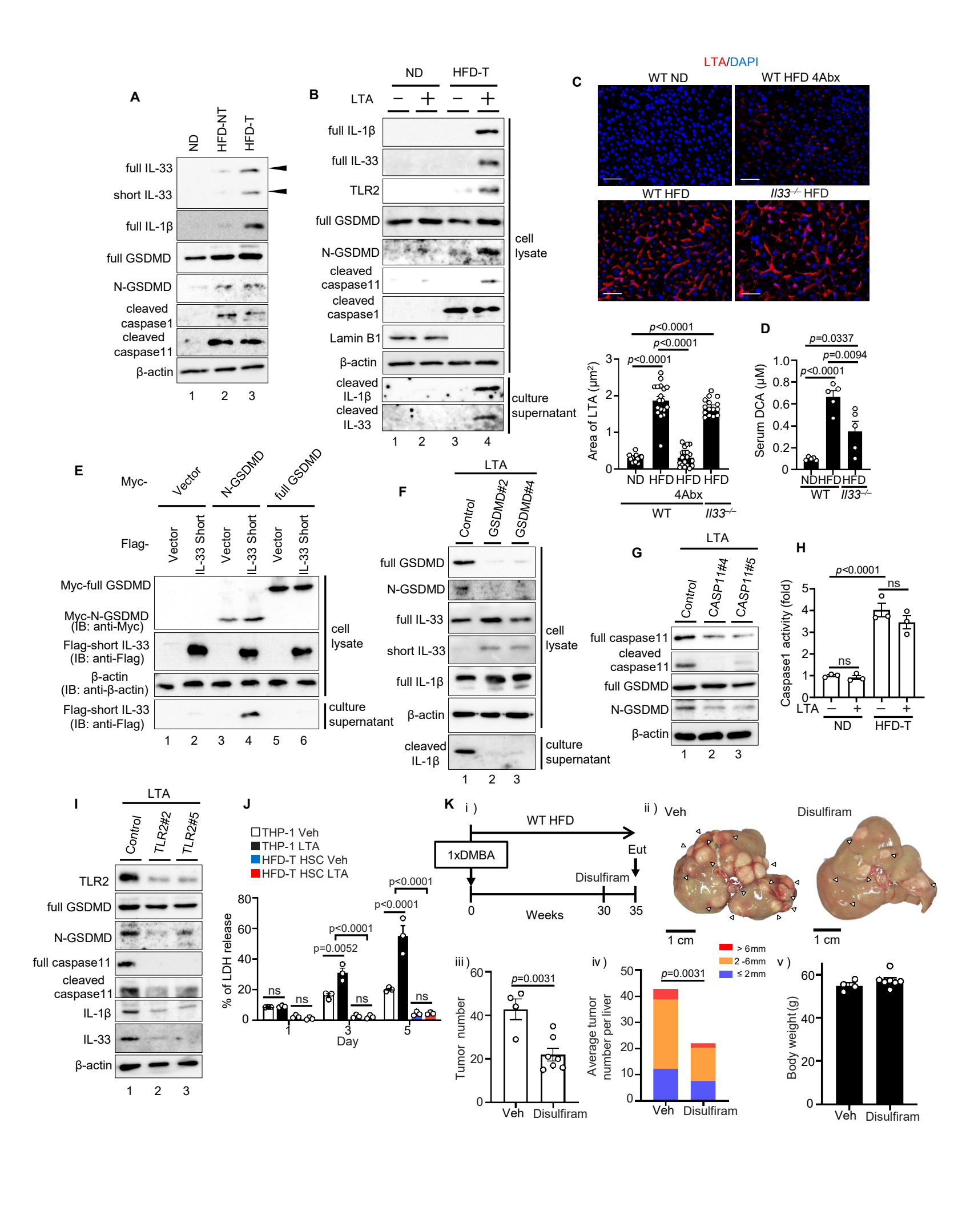
A
ND
HFD-NT
HFD-T
full IL-33
short IL-33
full IL-1β
full GSDMD
N-GSDMD
cleaved caspase1
cleaved caspase11
β-actin
1 2 3
B
ND
HFD-T
LTA
full IL-1β
full IL-33
TLR2
full GSDMD
N-GSDMD
cleaved caspase11
cleaved caspase1
Lamin B1
β-actin
cell lysate
cleaved IL-1β
cleaved IL-33
culture supernatant
1 2 3 4
C
LTA/DAPI
WT ND
WT HFD 4Abx
WT HFD
Il33−/− HFD
Area of LTA (μm²)
p<0.0001
p<0.0001
p<0.0001
ND HFD HFD HFD
4Abx
WT Il33−/−
D
Serum DCA (μM)
p=0.0337
p=0.0094
p<0.0001
ND HFD HFD
WT Il33−/−
E
Myc-
Vector
N-GSDMD
full GSDMD
Flag-
Vector
IL-33 Short
Myc-full GSDMD
Myc-N-GSDMD (IB: anti-Myc)
Flag-short IL-33 (IB: anti-Flag)
β-actin (IB: anti-β-actin)
cell lysate
Flag-short IL-33 (IB: anti-Flag)
culture supernatant
1 2 3 4 5 6
F
LTA
Control
GSDMD#2
GSDMD#4
full GSDMD
N-GSDMD
full IL-33
short IL-33
full IL-1β
β-actin
cell lysate
cleaved IL-1β
culture supernatant
1 2 3
G
LTA
Control
CASP11#4
CASP11#5
full caspase11
cleaved caspase11
full GSDMD
N-GSDMD
β-actin
1 2 3
H
Caspase1 activity (fold)
p<0.0001
ns
ns
LTA
ND
HFD-T
I
LTA
Control
TLR2#2
TLR2#5
TLR2
full GSDMD
N-GSDMD
full caspase11
cleaved caspase11
IL-1β
IL-33
β-actin
1 2 3
J
THP-1 Veh
THP-1 LTA
HFD-T HSC Veh
HFD-T HSC LTA
% of LDH release
p<0.0001
p<0.0001
p=0.0052
ns
ns
ns
ns
Day
K
i)
WT HFD
1xDMBA
Eut
Disulfiram
0
Weeks
30
35
ii) Veh
Disulfiram
1 cm
1 cm
iii)
Tumor number
p=0.0031
Veh
Disulfiram
iv)
Average tumor number per liver
p=0.0031
> 6mm
2 -6mm
≤ 2mm
Veh
Disulfiram
v)
Body weight (g)
Veh
Disulfiram

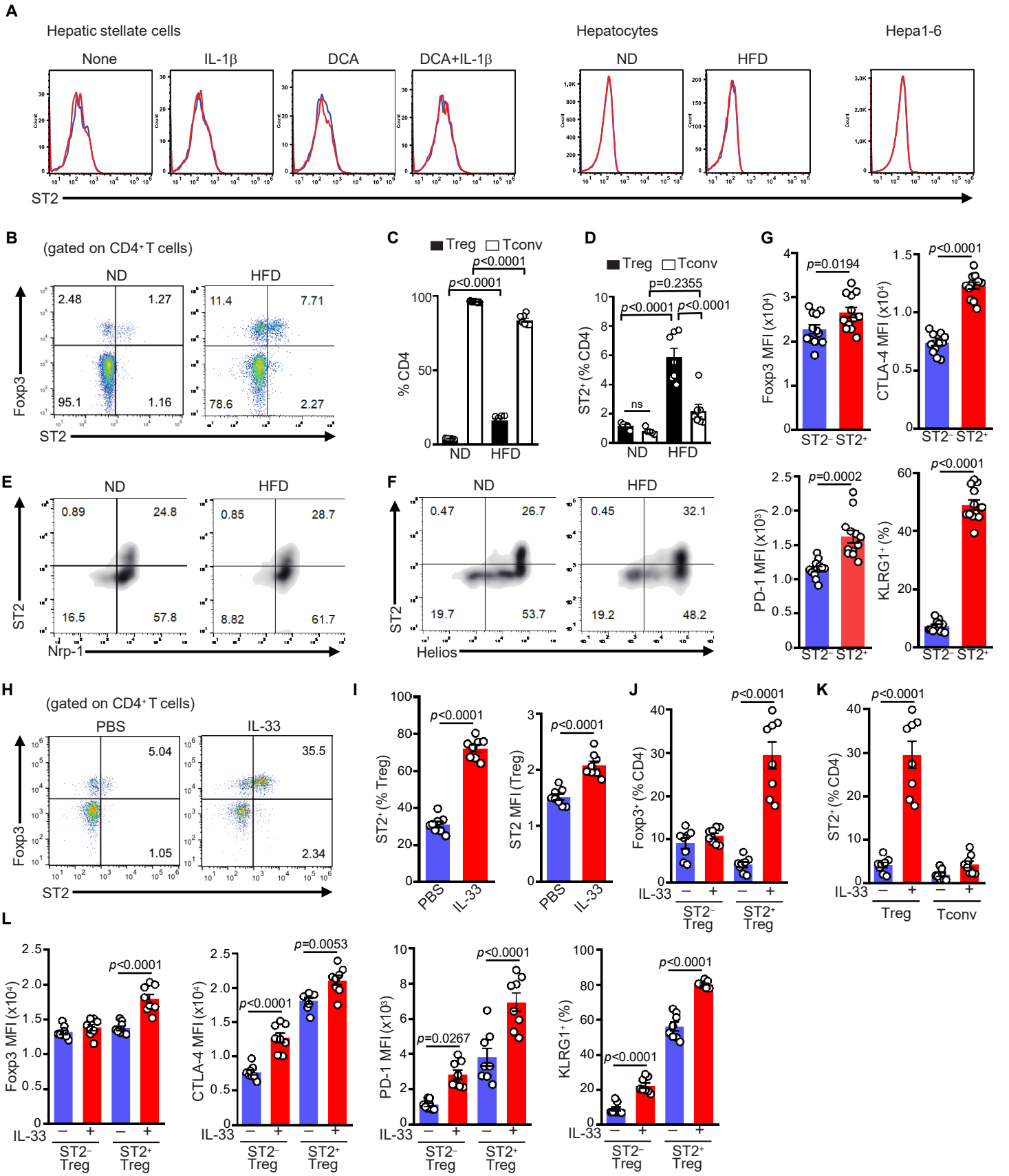
A
Hepatic stellate cells
None
IL-1β
DCA
DCA+IL-1β
Hepatocytes
ND
HFD
Hepa1-6
ST2
B
(gated on CD4⁺ T cells)
ND
HFD
2.48
1.27
95.1
1.16
11.4
7.71
78.6
2.27
Foxp3
ST2
C
Treg
Tconv
p<0.0001
p<0.0001
% CD4
ND
HFD
D
Treg
Tconv
p=0.2355
p<0.0001
p<0.0001
ns
ST2⁺ (% CD4)
ND
HFD
G
p=0.0194
Foxp3 MFI (x10⁴)
ST2⁻ ST2⁺
p<0.0001
CTLA-4 MFI (x10⁴)
ST2⁻ ST2⁺
E
ND
HFD
0.89
24.8
16.5
57.8
0.85
28.7
8.82
61.7
ST2
Nrp-1
F
ND
HFD
0.47
26.7
19.7
53.7
0.45
32.1
19.2
48.2
ST2
Helios
p=0.0002
PD-1 MFI (x10³)
ST2⁻ ST2⁺
p<0.0001
KLRG1⁺ (%)
ST2⁻ ST2⁺
H
(gated on CD4⁺ T cells)
PBS
IL-33
5.04
35.5
1.05
2.34
Foxp3
ST2
I
p<0.0001
ST2⁺ (% Treg)
PBS
IL-33
p<0.0001
ST2 MFI (Treg)
PBS
IL-33
J
p<0.0001
Foxp3⁺ (% CD4)
IL-33
ST2⁻ Treg
ST2⁺ Treg
K
p<0.0001
ST2⁺ (% CD4)
IL-33
Treg
Tconv
L
p<0.0001
Foxp3 MFI (x10⁴)
IL-33
ST2⁻ Treg
ST2⁺ Treg
p=0.0053
p<0.0001
CTLA-4 MFI (x10⁴)
IL-33
ST2⁻ Treg
ST2⁺ Treg
p<0.0001
p=0.0267
PD-1 MFI (x10³)
IL-33
ST2⁻ Treg
ST2⁺ Treg
p<0.0001
p<0.0001
KLRG1⁺ (%)
IL-33
ST2⁻ Treg
ST2⁺ Treg

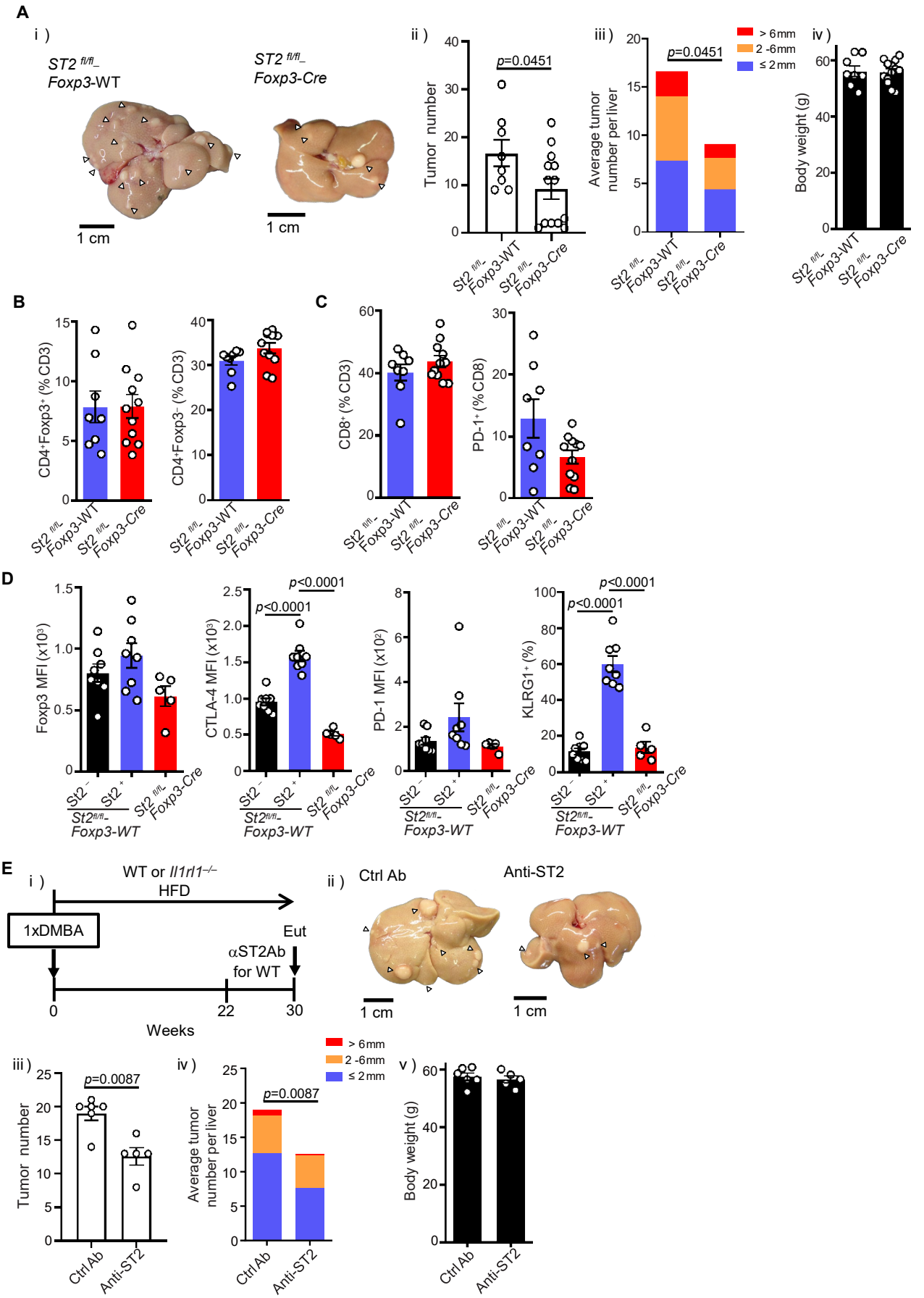
A
i)
ST2 fl/fl_ Foxp3-WT
ST2 fl/fl_ Foxp3-Cre
1 cm
1 cm
ii)
p=0.0451
Tumor number
St2 fl/fl- Foxp3-WT
St2 fl/fl- Foxp3-Cre
iii)
p=0.0451
> 6mm
2 -6mm
≤ 2mm
Average tumor number per liver
iv)
Body weight (g)
B
CD4+Foxp3+ (% CD3)
CD4+Foxp3- (% CD3)
C
CD8+ (% CD3)
PD-1+ (% CD8)
D
Foxp3 MFI (x10³)
CTLA-4 MFI (x10³)
p<0.0001
PD-1 MFI (x10²)
KLRG1+ (%)
St2- St2fl/fl-Foxp3-WT
St2+ St2fl/fl-Foxp3-WT
St2 fl/fl- Foxp3-Cre
E
i)
WT or Il1rl1-/- HFD
1xDMBA
Eut
αST2Ab for WT
0
22
30
Weeks
ii)
Ctrl Ab
Anti-ST2
1 cm
1 cm
iii)
p=0.0087
Tumor number
CtrlAb
Anti-ST2
iv)
p=0.0087
> 6mm
2 -6mm
≤ 2mm
Average tumor number per liver
v)
Body weight (g)

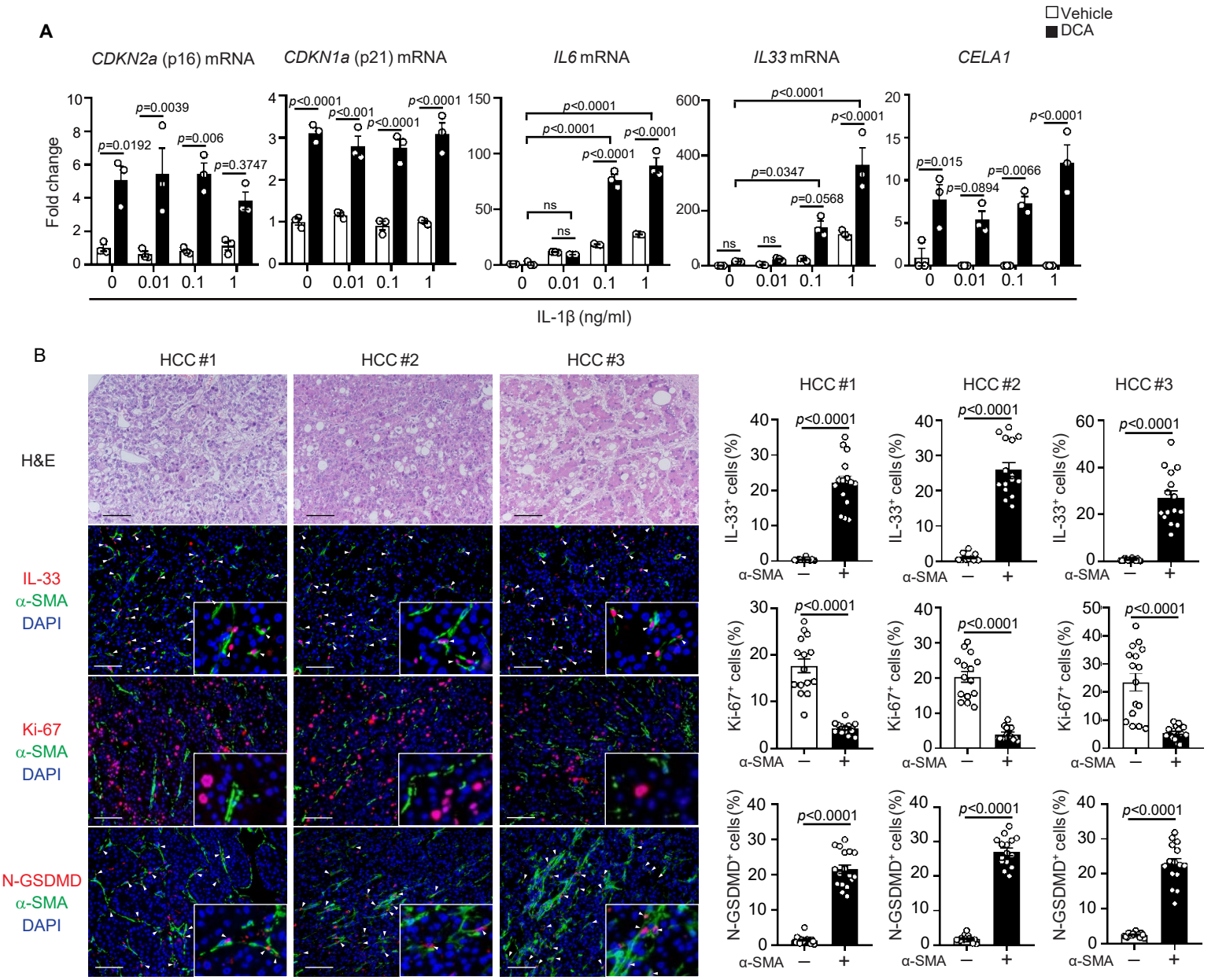

C

No	1	2	3
Age	74	67	71
Sex (male / female)	male	male	male
BMI	29.2	24.2	24.2
Diabetes (yes / no)	yes	yes	yes
Histological grading	Moderate	Moderate	Moderate

Supplementary Materials for

Gasdermin D-mediated release of IL-33 from senescent hepatic stellate cells promotes obesity-associated hepatocellular carcinoma

Ryota Yamagishi, Fumitaka Kamachi, Masaru Nakamura, Shota Yamazaki, Tomonori Kamiya, Masaki Takasugi, Yi Cheng, Yoshiki Nonaka, Yoshimi Yukawa-Muto, Le Thi Thanh Thuy, Yohsuke Harada, Tatsuya Arai, Tze Mun Loo, Shin Yoshimoto, Tatsuya Ando, Masahiro Nakajima, Hayao Taguchi, Takamasa Ishikawa, Hisaya Akiba, Sachiko Miyake, Masato Kubo, Yoichiro Iwakura, Shinji Fukuda, Wei-Yu Chen, Norifumi Kawada, Alexander Rudensky, Susumu Nakae, Eiji Hara, and Naoko Ohtani

***Corresponding author. Naoko Ohtani**

Email: naoko.ohtani@omu.ac.jp

This file includes:

Other Supplementary Materials for this manuscript include the followings:

Materials and Methods

Cell culture

Primary murine HSCs and the primary human HSC cell line, LI90 (JCRB0160), were cultured in Dulbecco's modified Eagle's medium supplemented with 10% fetal bovine serum in 5% O_2 and 5% CO_2 conditions. Primary murine HSCs were cultured in the absence or presence of DCA (250 μM) for 8 days and then were treated with IL-1b (Milteny Biotec). LI90 cells were cultured in the absence or presence of DCA (250 μM) for 15 days and then were treated with IL-1b (BioLegend). The murine hepatocellular carcinoma cell line, Hepa1-6, was obtained from DS Pharma Medical. Hepa1-6 and HEK293T cells were cultured in Dulbecco's modified Eagle's medium supplemented with 10% fetal bovine serum in 20% O_2 and 5% CO_2 conditions. No mycoplasma contamination was detected in the cells used in this study.

Quantitative PCR

Total RNA was extracted from mouse tissues or cultured murine cells using TRIzol (Thermo Fisher) and reverse transcription was performed using PrimeScript™ RT Master Mix (TakaraBio) according to manufacturer's instructions. Total RNA from human HSCs was used for "gene-specific" reverse transcription using PrimeScript II Reverse Transcriptase (TakaraBio) and the gene-specific primers are shown in Table S1. Quantitative PCR was performed using TB Green® Premix Ex Taq™ II (TakaraBio). The qPCR conditions were 95℃ for 30 sec; followed by 40 cycles of 95℃ for 5 sec and 60℃ for 30 sec. Expression levels of target genes were normalized to the expression of the *Gapdh*. Primers used for cDNA amplification are shown in Table S1. Representative data of two to three independent experiments are shown in the figures.

Recombinant IL-33 protein for cell-free digestion

For the use of in vitro digestion by CELA-1 in Fig 3F was created as follows. The nucleotide sequence of full-sized murine IL-33 with flanking NdeI and XhoI restriction sites was cloned into the E. coli expression vector pColdI (TakaraBio). Plasmid construction is shown in Fig. S9 in the supplementary material. To expand the expression of recombinant protein, the mIL-33-pColdI expression vector was transformed into ArcticExpress Competent Cells (Agilent Technology). The purification of recombinant IL-33 was performed according to the manufacturer's protocol with refolding by dialysis and used for in vitro digestion by CELA-1 in Fig. 3F.

Quantitative PCR for *Firmicutes* genome DNA

Bacterial DNA extraction from the stool of wild type (WT) mouse or IL-33 KO mouse was carried out by BIKEN Biomics Inc. (Osaka, Japan) using an automated DNA extraction machine (GENE PREP STAR PI-480, Kurabo Industries Ltd., Osaka, Japan) and NR-201 DNA extraction kit (Kurabo Industries Ltd., Osaka, Japan). Quantitative PCR was performed using TB Green® Premix Ex Taq™ II (TakaraBio). The qPCR conditions were 95℃ for 30 sec; followed by 40 cycles of 95℃ for 5 sec and 60℃ for 30 sec. Amounts of *Firmicutes* genome DNA were normalized to all *Bacteria* genome. Primers used for DNA amplification are shown in Table S1. Representative data of two independent experiments are shown in the figures.

Western blot analysis

Tissue or cell lysates were prepared in lysis buffer (50 mM HEPES (pH7.5), 150 mM NaCl, 1 mM EDTA, 2.5 mM EGTA, 10% glycerol, 0.1% Tween 20 and 10 mM β-glycerophosphate) containing a protease inhibitor cocktail (Nacalai tesque) using a homogenizer. The transferred membranes were immunoblotted directly with antibodies

shown in Table S1, and the signals were detected using an enhanced chemiluminescence system (GE Healthcare) and/or Can Get signal (TOYOBO).

SA-β-galactosidase assay

Primary HSCs were cultured in Dulbecco's modified Eagle's medium supplemented with 10% fetal bovine serum for 2 days. The cells were washed 2 times with phosphate-buffered saline (PBS) and fixed 4% paraformaldehyde in PBS for 5 min. After 2 times washing with PBS, the cells were stained with staining solution (40 mM Citric acid-Sodium phosphate buffer (pH 6.0), 5 mM K4[Fe(CN)6]3H2O, 5 mM K3[Fe(CN)6], 150 mM NaCl, 2mM MgCl2, 1mg/ml X-gal) for 16 hours at 37℃. After 2 times washing with PBS, the cells were counted under microscope.

Cell proliferation assay

Cells were cultured on 10 cm dishes with 1 mm grids (IWAKI) in the absence or presence of LTA. The number of cells in each grid was counted, and the relative number of cells was calculated based on an adjusted cell number at day 0 set at 1.0.

Immunoprecipitation

HSCs culture supernatants were incubated for 5 hours at 4℃ with anti-mIL-33 antibody (R&D Systems) and Dynabeads^{TM} Protein G (Thermo Fisher), and the beads were washed five times with 0.1% Tween-20 in PBS. Bound protein was eluted by SDS-PAGE sample buffer and analyzed by western blotting.

ELISA

Serum CD14 level was measured by Mouse CD14 Quantikine ELISA Kit (R&D Systems) following manufacturer instructions.

Generation of anti-mouse ST2 mAb

The anti-mouse ST2 mAb was generated by immunizing Sprague Dawley rat with

recombinant mouse ST2 Fc chimera (R&D Systems;1004-MR), consisting of the extracellular domains of mouse ST2 (Ser27 - Ser342) and the Fc portion of human IgG1 (Pro100 - Lys330). Three days after the final immunization, lymph node cells were fused with P3U1 myeloma cells. After hypoxanthine-aminopterin-thymidine selection, a hybridoma-producing anti-ST2 mAb (rat IgG2a, k) was selected based on its reactivity to ST2-transfected L5178Y cells, but not to parental L5178Y cells by flow cytometry and the cloned by limiting dilution. The inhibitory function of the anti-ST2 mAb was evaluated by its ability to inhibit the IL-6 production from IL-33-stimulated mast cells. The IL-6 production was measured by ELISA using culture supernatants of bone marrow-derived mast cells (BMMCs) treated with 0.5 ng/ml of recombinant IL-33 (eBioscience;34-8332) in the presence of 10 mg/ml of anti-ST2 mAb or control rat IgG. BMMCs were prepared by culturing bone marrow cells isolated from BALB/c mice and cultured for 4-6 weeks in RPMI1640 medium containing 10% FBS, 0.1 mg/ml penicillin and streptomycin, 100 mM 2-mercaptoethanol, 10 mM sodium pyruvate, 10 mM minimum essential medium nonessential amino acids solution, 10 mM HEPES, 10 ng/ml recombinant murine IL-3, and 10 ng/ml recombinant stem cell factor. Flow cytometric analysis identified more than 95% of cells like mast cells (KIT^+ $FceRI^+$). The inhibitory effect of the antibody is verified, and we confirmed 83% inhibitory effect of IL-6 production from bone marrow-derived mast cells.

Supplementary Figures

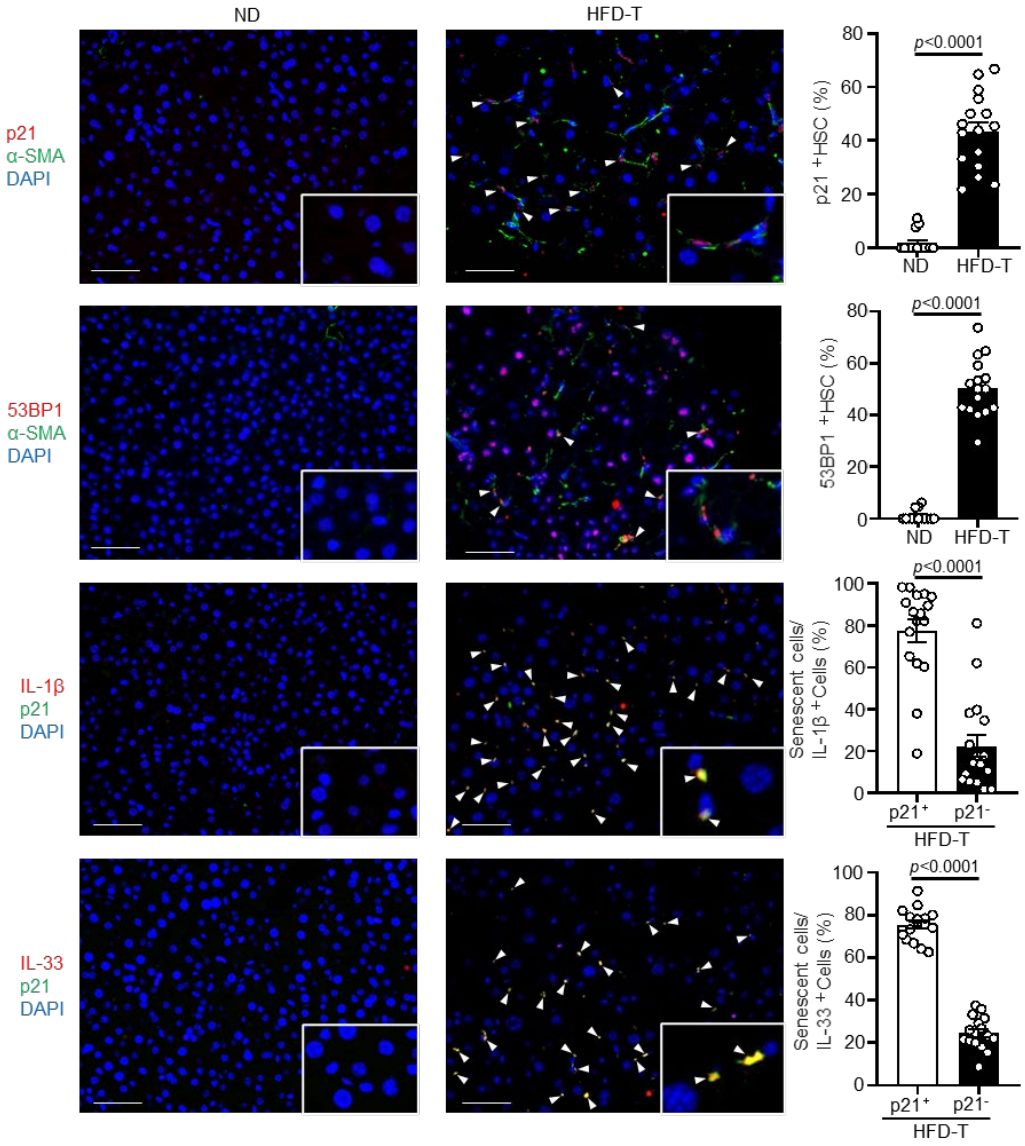

Fig. S1. HSCs in the tumor microenvironment of HFD-fed mice show a senescent phenotype.

Immunofluorescence staining of liver section from DMBA-treated and ND-fed and DMBA-treated and HFD-fed WT mice. HSCs were visualized by α-SMA staining (green) and the cell nuclei were stained by 4,6-diamidino-2-phenylindole (DAPI; blue). Arrowheads indicate α-SMA expressing cells that were positive for indicated markers (red). The histograms indicate the percentages of α-SMA-expressing cells that were positive for 53BP1 or p21, and the percentages of $p21^+$ or $p21^-$ cells that were positive for IL-1b or IL-33 (p21 expression is used as a senescence marker). Scale bars, 50 μm. T; tumor cell. HSC; hepatic stellate cell. Data of three mice in each group are represented and at least 100 cells were counted per group for statistical analysis. All graphs represent mean ± SEM. The indicated *p* values were calculated by Mann-Whitney test. ND: normal diet-fed mouse liver, HFD-T: high fat diet-fed mouse liver tumor.

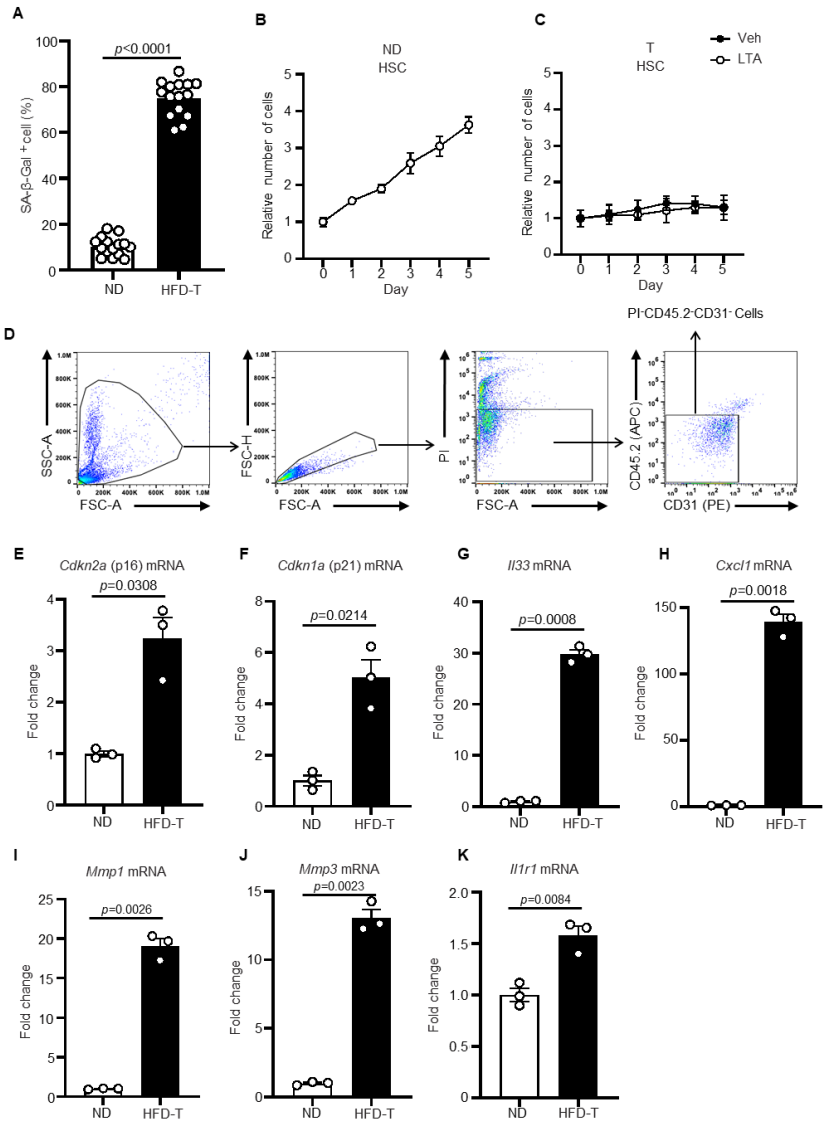

Fig. S2. The markers of cellular senescence and SASP are upregulated in HSCs from HFD-induced tumor region.

A, Cell counts positive for SA-b galactosidase activity staining. **B and C,** Cell growth curve of isolated primary HSCs. Relative cell numbers counted every day for five days are shown. Relative cell counts of HSCs from ND-fed mouse liver (b) and from HFD-fed mice with or without the LTA treatment (c). **D,** Representative flow cytometry plots and gating strategy for sorting of HSCs from livers of wild type DMBA-treated HFD-fed mice, related to Fig. 4 and panel E to K. Gating strategy for sorting is shown. The population of PI-CD45.2-CD31- cells were sorted as HSCs. The detailed information for HSC isolation from the liver is described in the Method section. **E to K,** The freshly isolated HSCs from DMBA-treated ND or HFD-fed mouse livers were subjected to qPCR for *CDKN2a* (p16) **(E)**, *CDKN1a* (p21) **(F)**, *Il33***(G)**, *Cxcl1***(H)**, *Mmp1***(I),** *Mmp3* **(J)** or *Il1R1* **(K)** gene expression. All graphs represent mean ± SEM. The indicated *p* values were calculated by Welch's t-test. ND: normal diet-fed mouse liver, HFD-T: high fat diet-fed mouse liver tumor.

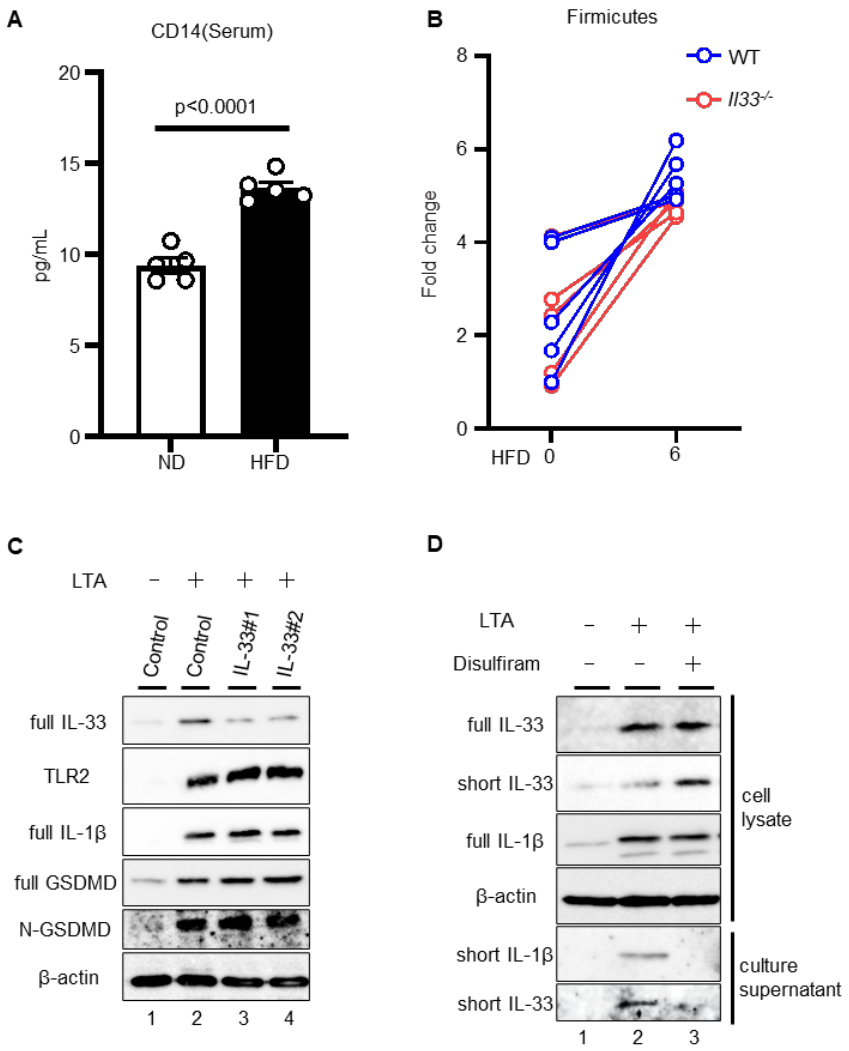

Fig. S3. IL-33 deficiency does not affect the LTA-TLR2 signaling

A, Serum CD14 levels were evaluated by ELISA. DMBA-treated ND-fed (n=5) or HFD-fed (n=5) WT mice. All graphs represent mean ± SEM. The indicated *p* values were calculated by Student's two-tailed unpaired *t* test. B, 10 weeks old wild type (WT) mouse or Il33$^{-/-}$ mouse were fed a high-fat diet (HFD) for 6 week. Bacterial DNAs were extracted from stool of wild type (WT) mouse or IL-33 KO mouse. The DNAs were subjecuted to qPCR for Firmicutes genome DNA. C, Freshly isolated murine primary HSCs from HFD-induced liver tumor region were infected with shRNA vectors targeting IL-33 or with control shRNA vector for 2 days, and then 25mg/ml LTA was added. After 24 hours, the cell extracts or culture supernatant were subjected to immunoblotting using antibodies shown on the left. D, Freshly isolated murine primary HSCs from HFD-induced liver tumor region were pretreated with 1 μM Disulfiram for 1 hour, and then 25mg/ml LTA was added. After 24 hours, the cell lysates or culture supernatant were subjected to western blotting using antibodies shown on the left.

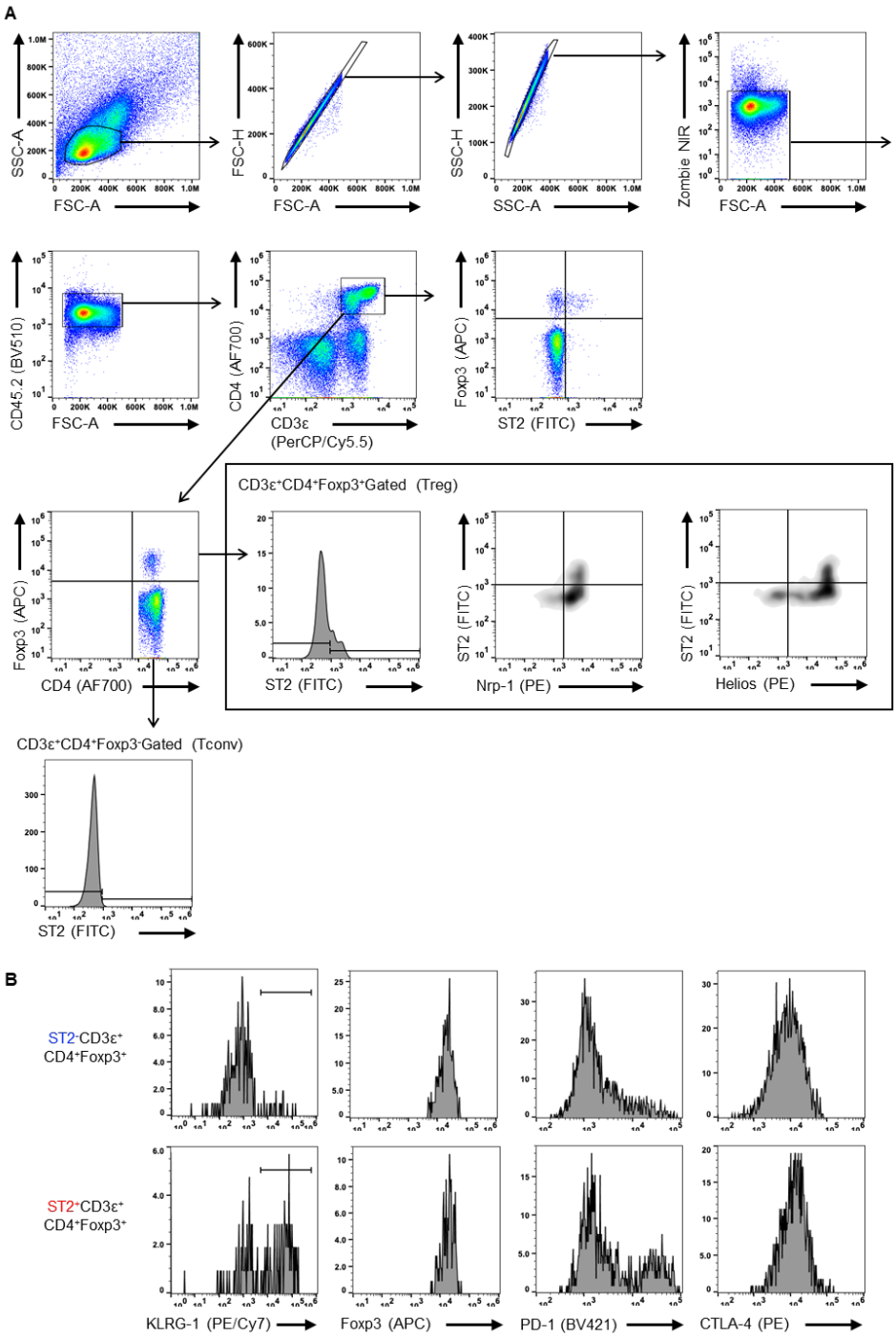

Fig. S4. Characterization of the Treg population from the liver of DMBA-treated mice.

A, B Representative flow cytometry plots, histograms and gating strategy by lymphocytes from livers of DMBA-treated mice, related to Figure 5 and 6. Gating strategy showing the population of surface ST2 and intracellular Foxp3 expression in CD3ε+ CD4+ cells (A). Histograms showing the expression of KLRG-1, Foxp3, PD-1 and CTLA-4 in ST2–CD3ε+CD4+Foxp3+ cells or in ST2+CD3ε+CD4+Foxp3+ cells (B).

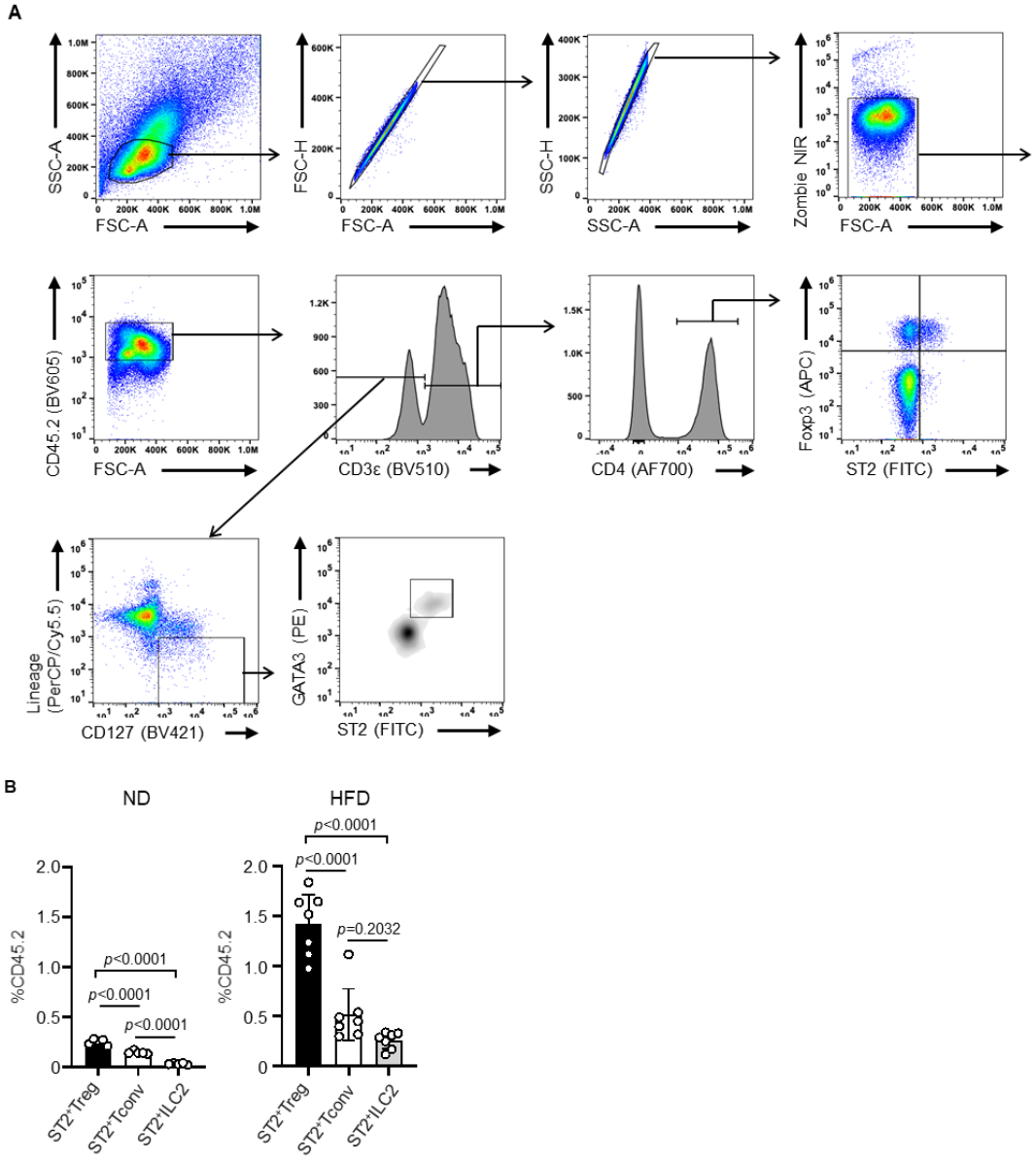

Fig. S5. Characterization of the ILC2 population from the liver of DMBA-treated mice.

Flow cytometric analysis of ST2-positive lymphocytes from livers of ND-fed (n=5) or HFD-fed (n=7) WT mice. **A,** Representative flow cytometry plots and gating strategy by lymphocytes from livers of DMBA-treated HFD-fed WT mice. Gating strategy showing the population. **B**, Frequency of $ST2^{+}Foxp3^{+}$ (Treg), $ST2^{+}Foxp3^{-}$ (Tconv) or $ST2^{+}Linege^{-}CD127^{+}GATA3^{+}$ (ILC2) among $CD45.2^{+}$ cells. All graphs represent mean ± SEM. The indicated *p*-values were calculated by one-way ANOVA with Bonferroni's multiple comparisons test.

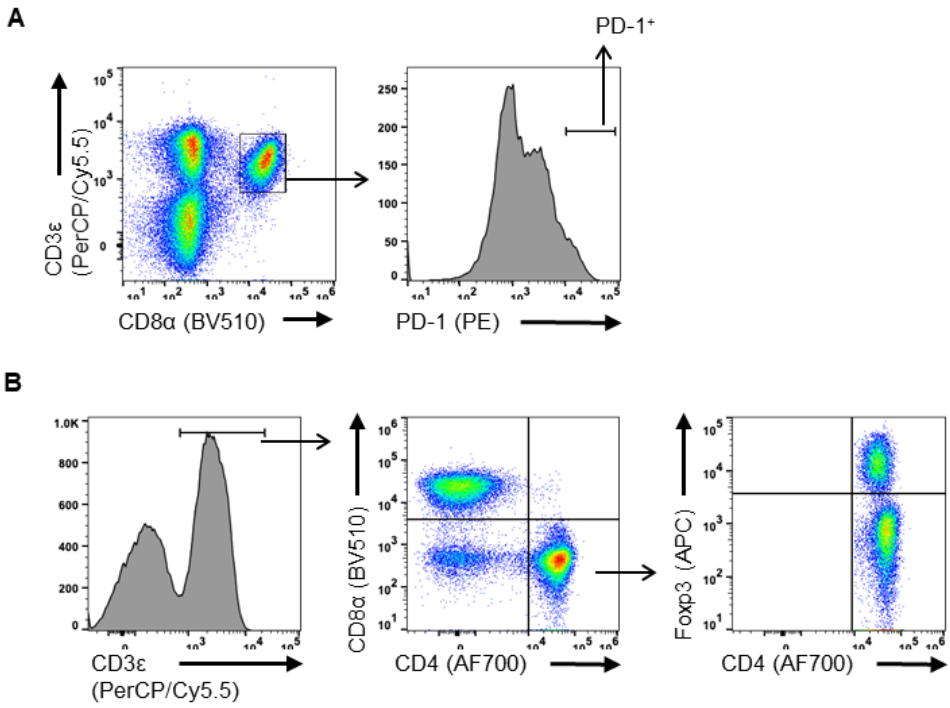

Fig. S6. Characterization of the T cell population from the liver of ST2$^{fl/fl}$-Foxp3Cre mice.

A, B Representative flow cytometry plots and gating strategy by lymphocytes from livers of DMBA-treated *ST2$^{fl/fl}$-Foxp3WT* and *ST2$^{fl/fl}$-Foxp3Cre* mice, related to Fig. 6. Gating strategy showing the population of surface PD-1 expression in CD3ε^{+}CD8a^{+} cells **(A)**. Gating strategy showing the population of CD3ε^{+}CD4^{+}Foxp3^{+} cells or CD3ε^{+}CD4^{+}Foxp3^{-} cells **(B)**.

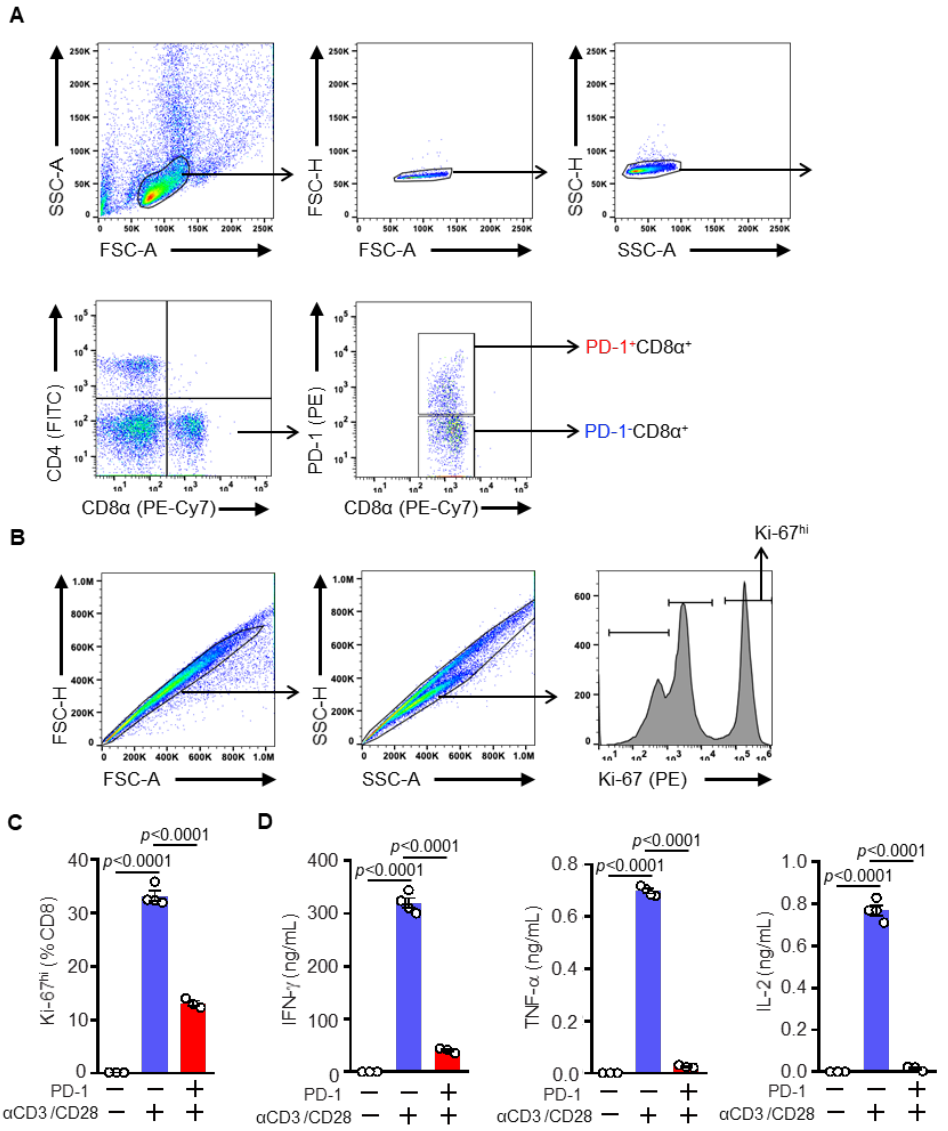

Fig. S7. Cytotoxic CD8+ T cells over-expressing PD-1 in tumor microenvironment show exhausted phenotypes in this mouse model.

A, B Representative flow cytometry plots and gating strategy by lymphocytes from livers of DMBA-treated HFD-fed WT mice. Gating strategy for sorting and showing the population of surface PD-1 expression in $CD3\varepsilon^{+}CD8a^{+}$ cells **(A)**. Gating strategy showing the expression of intracellular $Ki\text{-}67^{+}$ among $CD8^{+}$ cells **(B)**. **C, D** $PD\text{-}1^{-}$ $CD3\varepsilon^{+}CD8^{+}$ T cells and $PD\text{-}1^{hi}CD3\varepsilon^{+}CD8^{+}$ T cells were sorted from DMBA-treated HFD-fed WT mouse livers by cell sorter. Purified $CD8^{+}$ T cells were stimulated with plate-coated anti-CD3 mAb (145-2C11, 5 μg/mL) and soluble anti-CD28 mAb (37.51, 2.5μg/mL) for 3 days. Frequency of intracellular $Ki\text{-}67^{+}$ among $CD8^{+}$ cells were analyzed by flow cytometry **(C)**. Concentrations of IFN-γ, TNF-α, and IL-2 in culture supernatants were measured by ELISA **(D)**. All graphs represent mean ± SEM. The indicated *p* values were calculated by one-way ANOVA with Bonferroni's multiple comparisons test.

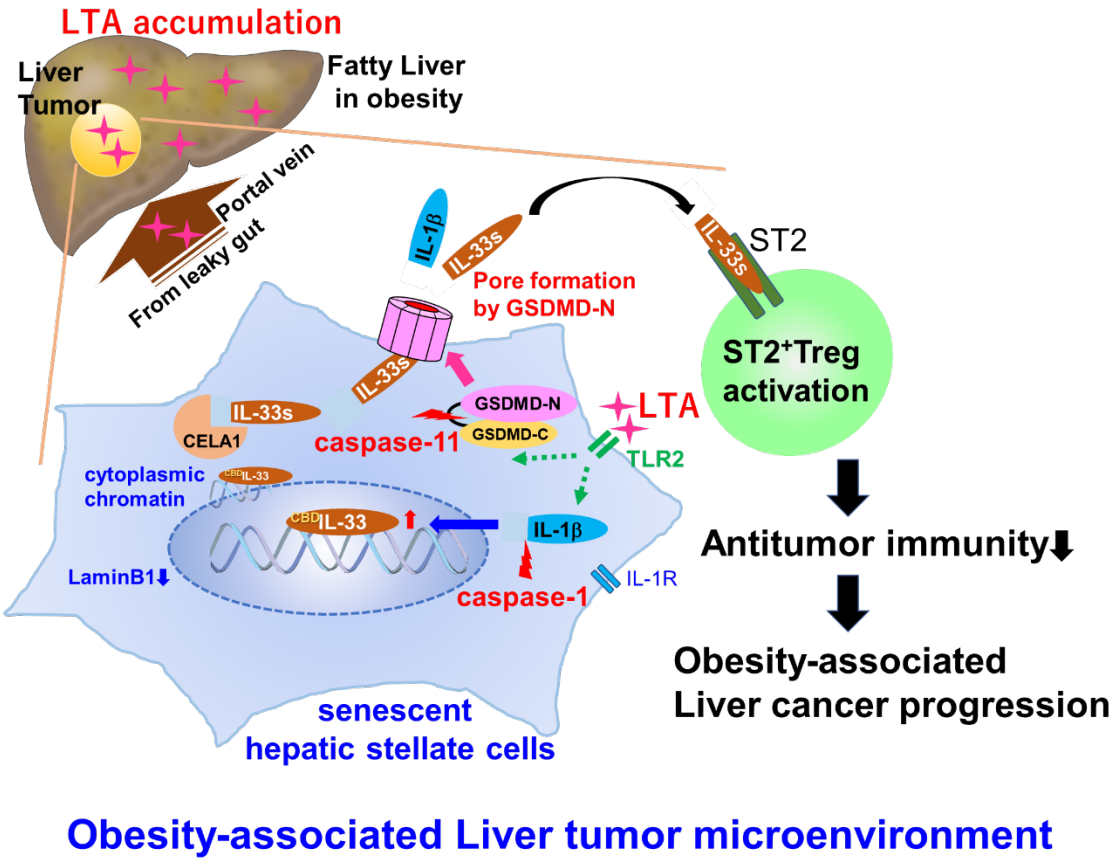

Fig. S8. Summary scheme of the present work: The release mechanism of IL-1b and IL-33 from senescent HSCs and their tumorigenic orchestration.
Hepatic stellate cells in obesity-associated liver tumor microenvironment exhibit cellular senescence and SASP with the upregulation of SASP factors, IL-33 and IL-1β and caspases -1 and -11. IL-1β is cleaved by caspase-1 to become an active form and can induces IL-33 expression. A certain amount of chromatin-bound IL-33 emerge to cytoplasm due to fragile nuclear membrane by the downregulation of Lamin B1, which is a characteristic of senescent cells. CELA1 can cleave cytoplasmic IL-33 to create its short and active form. The obesity-associated liver tissue is highly exposed to LTA, a cell wall component of obesity-increased Gram-positive gut microbiota. LTA stimulation activate caspse-11 to create GSDMD N-terminus. The short and active forms of IL-1b and IL-33 were released from LTA-stimulated senescent HSCs through the cell membrane pore formed by the GSDMD N-terminus, promoting obesity-associated hepatocellular carcinoma (HCC) development via ST2-positive Treg cell activation by IL-33. This novel release mechanism of IL-1b and IL-33 from senescent HSCs facilitates tumorigenic orchestration.

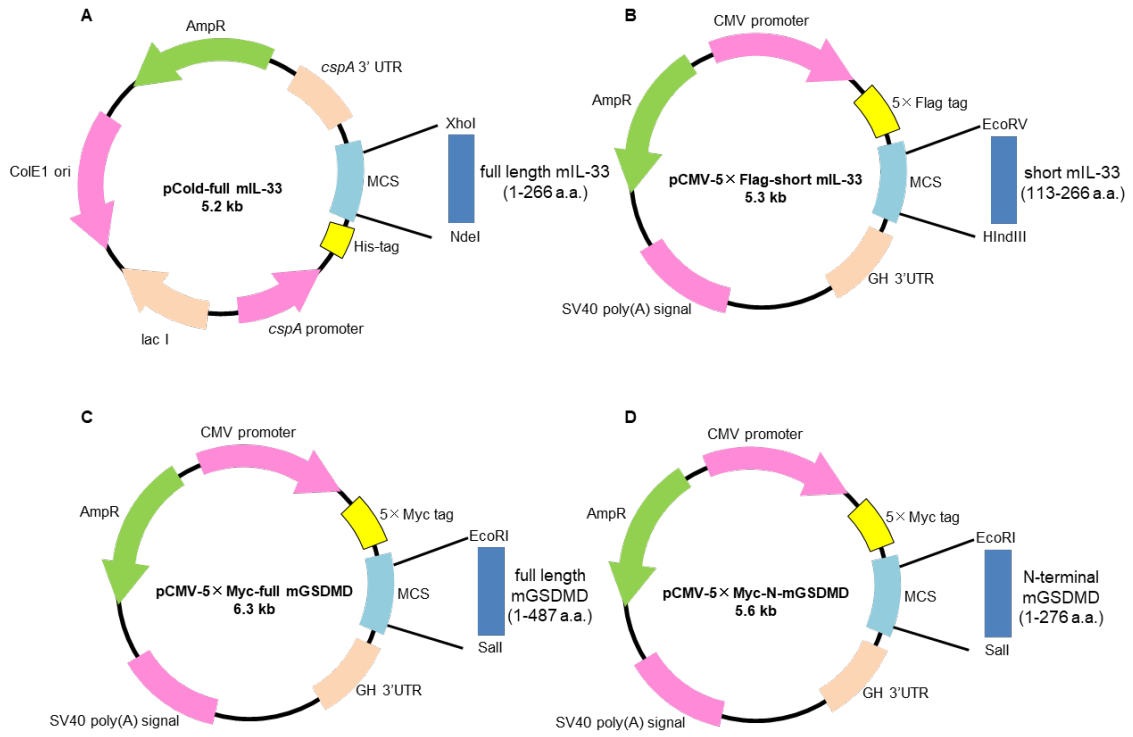

Fig. S9. The maps of plasmids constructed in this study.
A, pCold-full mIL-33. **B,** pCMV-5×Flag-short form of mIL-33. **C,** pCMV-5×Myc-full mGSDMD. **D,** pCMV-5×Myc-N-mGSDMD. GH: growth hormone gene.

Other Supplementary Materials for this manuscript include the followings:

Fig. S10. Full gel scans for Western blotting data.

Table S1. The list of antibodies and primers used in this study

Table S2. Reagents for isolating hepatic stellate cells from mouse livers

Table S3. Raw data for graphs and statistics